1   An offset in TEX$_{86}$ values between interbedded lithologies: implications for

2   sea-surface temperature reconstructions

3

4   Kate Littler[a,b*], Stuart A. Robinson[a,c], Paul. R. Bown[a]

5

6   *a*Department of Earth Sciences, University College London, Gower Street, London, WC1E

7   6BT, UK.

8   *b*Now at: Camborne School of Mines, University of Exeter, Penryn Campus, Cornwall.

9   TR10 9EZ, UK.

10   *c*Now at: Department of Earth Sciences, University of Oxford, South Parks Road, Oxford,

11   OX1 3AN, UK

12   *Corresponding author. E-mail address:* k.littler@exeter.ac.uk (K. Littler)

13

14   ABSTRACT

15   The TEX$_{86}$ (TetraEther indeX of tetraethers consisting of 86 carbon atoms) sea-surface

16   temperature (SST) proxy is based on the distribution of isoprenoid glycerol dialkyl glycerol

17   tetraether (GDGT) membrane lipids of pelagic Thaumarchaeota that are preserved in marine

18   sediments. It is a valuable tool for reconstructing past SSTs from sedimentary archives,

19   however there are still major uncertainties as to the effects of variables other than

20   temperature on the proxy. Here we present the first study of GDGT variability across early

21   Cretaceous interbedded pelagic and shelf-sourced turbiditic sediments from two Deep Sea

22   Drilling Project (DSDP) sites in the western North Atlantic. The results indicate that a small,

23   but consistent, offset in TEX$_{86}$ ratios, equivalent to ~1–2°C of temperature difference,

24   occurs between interbedded lithologies of a similar age. The offset can be attributed to

25   spatial differences in sea-surface temperatures or thaumarchaeotal populations between the

26   shelf and the open ocean, or to secondary diagenetic effects related to oxic degradation of

27   the GDGTs. Of these, a difference in either thaumarchaeotal taxa or ecology between those

28   living in the shelf and ocean areas seems most plausible. Regardless of the root cause of the

29   offset, these findings highlight the necessity of careful sample selection prior to TEX_{86}

30   analysis, to ensure robust interpretation of palaeotemperature trends.

31

34

1. Introduction

1.1. The TEX_{86} proxy

37   TEX_{86} (TetraEther indeX of tetraethers consisting of 86 carbon atoms) is an organic

38   palaeotemperature proxy that has been used to reconstruct SSTs from sediments of Middle

39   Jurassic and younger age (e.g., Schouten et al., 2002; Littler et al. 2011; Jenkyns et al.,

40   2012; Schouten et al., 2013). The technique makes use of the relationship between the ratio

41   of different core GDGT lipids (without their polar head groups) synthesized by marine

42   Thaumarchaeota (previously "Marine Group I Crenarchaeota"; see Brochier-Armanet et al.,

43   2008), which varies according to the temperature of the seawater in which the organisms

44   live (Schouten et al., 2002, 2013). These pelagic GDGTs are exported to the seafloor where

45   they are thought to be stable on the timescale of thousands to millions of years (Schouten et

46   al., 2002, 2004; Sinninghe Damsté et al., 2002; Kim et al., 2009b). The application of

47   modern core-top calibrations (Schouten et al., 2002; Kim et al., 2008; 2010) to sedimentary

48   records allows the average temperature of past surface oceans to be determined. The TEX_{86}

49   proxy is therefore a powerful tool in the reconstruction of past climates, particularly where

50   traditional calcite-based palaeotemperature proxies cannot be applied with confidence, for

51 example in the low-carbonate settings of the high latitudes (e.g., Sluijs et al., 2006) or in

52 deeply buried, carbonate-rich sediments prone to diagenetic alteration (e.g., Littler et al.,

53 2011).

54   TEX_{86} ratios in modern core-top sediments have been shown empirically to best

55 correlate with mean annual average sea-surface temperature (maSST) at the site of

56 deposition, (e.g., Schouten et al., 2002; Kim et al., 2008; Wuchter et al., 2005, 2006b),

57 although a season-specific correlation with either winter or summer surface temperatures

58 cannot be ruled-out on the basis of the latest core-top dataset (Kim et al., 2010). Several

59 studies have also shown that core GDGTs in open-ocean marine sediments are more labile

60 and thus less subject to long-distance lateral advection than other organic molecules, such as

61 n-alkanes and alkenones, thus giving confidence in their utility for site-specific maSST

62 reconstructions (Mollenhauer et al., 2007, 2008; Shah et al., 2008; Kim et al., 2009a).

63 However, there is still much to learn about the ecology of the Thaumarchaeota themselves,

64 whose very existence only came to light 20 years ago, and whose important role in global

65 biogeochemical cycles as ammonia-oxidizers is still being explored (e.g., Furhman et al.,

66 1992; De Long, 1992; Ouverney and Fuhrman, 2000; Pearson et al., 2001; Könneke, et al.,

67 2005; Francis et al., 2005; Martens-Habbena et al., 2009; Stahl and de la Torre, 2012). With

68 regard to the fidelity of the TEX_{86} proxy, there are also uncertainties regarding both the

69 depth habit and seasonality preferences of the source organisms, and the possible additional

70 contribution of GDGTs from production sources in deeper water or the sedimentary

71 environment (e.g., Murray et al., 1998; Karner et al., 2001; Wuchter et al., 2005, 2006b;

72 Herfort et al., 2006; Ingalls et al., 2006; Huguet et al., 2007a; Mincer et al., 2007; Shah et

73 al., 2008; Weijers et al., 2011; Lengger et al., 2012).

74   The long-term persistence of the core GDGTs has been demonstrated by records

75 stretching back at least 160 million years (Middle Jurassic, e.g., Jenkyns et al., 2012).

76   However, to-date there has been no systematic investigation into the distribution of core

77   GDGTs in different lithologies within the marine environment, in sediments older than the

78   Miocene (Menzel et al., 2006; Huguet et al., 2009). The results of the Neogene studies show

79   that GDGT distributions can vary with lithology, but the explanation for this variability

80   ranges from biological and oceanographic (Menzel et al., 2006) to diagenetic (Huguet et al.,

81   2009), suggesting a complex mixture of controls that may influence TEX_{86} values in ancient

82   sediments. Understanding the magnitude and direction of such influences on TEX_{86} is

83   important, as deep-sea marine sediments frequently contain a mixture of authochthonous

84   pelagic deposits and allochthonous sediments transported from the shelf (e.g., Hsü et al.,

85   1974). If differences in TEX_{86} ratio do exist in different lithologies then this has

86   implications for sampling strategies and interpretations of maSST trends in palaeoclimate

87   reconstructions. The aim of this study is to explore the differences in TEX_{86} between

88   intercalated pelagic and transported early Cretaceous sediments from two western North

89   Atlantic DSDP sites (DSDP Sites 534 and 603; Fig. 1), in order to investigate the possible

90   effect of lithology on GDGT distribution and the TEX_{86} proxy.

91

92   **2. Materials and Methods**

93   *2.1. Early Cretaceous sediments from the western North Atlantic*

94   At DSDP Sites 534 and 603, Berriasian–Barremian (125–145 Ma) sediments

95   belonging to the Blake Bahama Formation are characterised by pelagic bioturbated chalks

96   and laminated marls interbedded with fine–medium grained, graded sandstones and

97   homogeneous mudstones. The latter lithologies are interpreted as allochthonous material

98   sourced from the adjacent shelf area, deposited by distal turbidites into the deep-sea (Fig. 2;

99   Sheridan et al., 1983; Robertson and Bliefnick, 1983; van Hinte et al., 1987). Here we focus

100   on laminated marls and homogeneous mudstones that are common throughout the

4

101   formation, and represent pelagic and transported deposition, respectively. The transported

102   mudstones can be regarded as having been deposited geologically instantaneously, and

103   therefore, when in close proximity to the pelagic marls are likely to be very similar in age.

104   The laminated, coccolith-rich, mid-grey marls were deposited in a fully open-ocean

105   setting, well above the calcite compensation depth (CCD) (Sheridan et al., 1983; Robertson

106   and Bliefnick, 1983; van Hinte et al., 1987). The sub-mm-scale laminations suggests

107   deposition in a largely dysoxic environment (Fig. 2), and are likely the result of cyclic

108   changes in clay input and/or periodic fluctuations in phytoplankton productivity in the

109   western North Atlantic during the early Cretaceous (Robertson and Bliefnick, 1983;

110   Robertson, 1984). By contrast, sedimentological, geochemical and micropalaeontological

111   evidence all indicates an allochthonous origin for the homogeneous mudstones (Sheridan et

112   al., 1983; Robertson and Bliefnick, 1983; van Hinte et al., 1987). The sharp basal contacts

113   are suggestive of energetic lateral emplacement of the mudstones, while the lack of laminae

114   suggests either intense bioturbation or turbulent mixing during deposition (Fig. 2; Sheridan

115   et al., 1983; Robertson and Bliefnick, 1983; Robertson, 1984; van Hinte et al., 1987).

116   Futhermore, at Site 603, there is a higher proportion of terrestrially-sourced organic matter

117   in the mudstones, as evidenced by geochemical data and the presence of woody fragments,

118   suggesting a more proximal origin for this lithology (Katz 1983; Herbin et al., 1983; Dean

119   and Arthur, 1987; Dunham et al., 1987). The composition of calcareous nannofossil

120   assemblages in the pelagic marls and homogeneous mudstones at Site 603 also indicate

121   different depositional origins, with a higher proportion of the shelf-dwelling *Nannoconus*

122   and *Micrantholithus* genera present in the mudstones (Covington and Wise, 1987;

123   Applegate et al., 1989; herein). No such observations have yet been made at Site 534.

124

125   *2.2. Sample collection and stratigraphy*

126   Pairs of Upper Berriasian to Upper Hauterivian samples were taken from DSDP Site

127   534, each consisting of a closely-spaced laminated marl and a homogeneous mudstone

128   sample, with a maximum offset of 73 cm and an average offset of 13 cm between each half

129   of the pair. Of the 23 pairs analysed, only 16 yielded sufficient GDGTs for TEX_{86} analysis.

130   Unfortunately, it was not possible to collect more pairs of samples due to to core disturbance

131   and a lack of sufficient GDGTs in some samples. In ten of the sixteen pairs, the

132   allochthonous mudstone was located stratigraphically above the pelagic marl (by an average

133   of 17 cm, maximum of 73 cm), ensuring samples of very similar geological age. This

134   equates to a maximum temporal offset between samples of ~34 kyrs (73 cm offset), a

135   minimum offset of ~0.25 kyrs (1 cm offset), and an average offset of ~4.2 kyrs (17 cm

136   offset), based on the age model used by Littler et al., (2011). At Site 603, thirty-nine

137   unpaired marl-mudstone samples from the lower Valanginian to upper Hauterivian were

138   analysed. These are not as closely-spaced as the samples from Site 534, but they provide

139   similar data in support of observations from Site 534. The stratigraphy of each site is based

140   on previous magnetostratigraphic and calcareous nannofossil biostratigraphic studies (Ogg,

141   1987; Bergen, 1994; Covington and Wise, 1987; Bornemann et al. 2008; Littler et al.,

142   2011).

143

144   *2.3. GDGT analysis and SST calibrations*

145   Powdered samples were solvent extracted and analysed according to the

146   methodology of Schouten et al. (2007). Samples were analysed using high-performance

147   liquid chromatography/atmospheric pressure positive ion chemical ionization mass

148   spectrometry (HPLC/APCI-MS), using an Agilent 1200 series LC/MSD SL, coupled to a

149   G6130A single quadrupole mass spectrometer (MS). The distribution of relevant core

150   GDGTs (Fig. S1) are considered in terms of both the TEX_{86}^{H} (high temperature calibration)

151   and TEX$_{86}$^{L} (low temperature calibration) indices (Equations 1 and 2), and, where

152   applicable, these distributions are converted to maSST estimates using Equations 3 and 4

153   (Kim et al. 2010):

154

155 $$TEX_{86}^{H} = \log\left(\frac{[GDGT\ 2]+[GDGT\ 3]+[GDGT\ 4']}{[GDGT\ 1]+[GDGT\ 2]+[GDGT\ 3]+[GDGT\ 4']} \right) \quad (1)$$

156

157 $$TEX_{86}^{L} = \log\left(\frac{[GDGT-2]}{[GDGT-1]+[GDGT-2]+[GDGT-3]} \right) \quad\quad (2)$$

158

159 $$SST = (68.4 * TEX_{86}^{H}) + 38.6 \quad\quad (3)$$

160

161 $$SST = (67.5 * TEX_{86}^{L}) + 46.9 \quad\quad (4)$$

162

163   Despite the high temperature nature of the Cretaceous SSTs, it was deemed necessary to

164   include the 'low temperature calibration', TEX$_{86}$^{L}, for completeness as this calibration

165   utilises different GDGTs and so may be sensitive to different environmental or ecological

166   differences between the two lithological types. Moreover, there is some controversy

167   regarding which is the most appropriate calibration to use in high temperature greenhouse

168   worlds, therefore inclusion of both calibrations is prudent (e.g., Hollis et al., 2012; Taylor et

169   al., 2013). Repeat analysis of an in-house standard and reference to previous work (Schouten

170   et al., 2007) suggests the analytical error associated with the TEX$_{86}$ technique using SIM

171   HPLC-MS techniques is ±0.012. This small analytical error equates to an error in maSST of

172   ±0.6 to 0.9°C (TEX$_{86}$^{H}) for the range of TEX$_{86}$ values in this study. However the standard

173   residual error (1σ) associated with the core-top calibration of Kim et al. (2010) is ±4 °C for

174   TEX$_{86}^{L}$ and ±2.5 °C for TEX$_{86}^{H}$. As no internal GDGT standard with a known GDGT

175   concentration was available, the isoprenoid GDGT relative concentrations are expressed as

176   the arbitrary abundance of GDGTs 1, 2, 3 and 4', scaled per gram of total bulk sediment

177   extracted, per μl of solvent introduced onto the HPLC column, and normalised to the

178   isoprenoid GDGT abundance of the internal standard for that analysis. The abundance of

179   branched GDGTs (GDGTs I, II and III) is expressed using the same normalisation method.

180   The BIT Index, a measure of the amount of terrestrial input to the marine

181   environment, was calculated after Hopmans et al., (2004) according to the equation:

182

183    $$BIT\ Index = \left(\frac{[GDGT - I] + [GDGT - II] + [GDGT - III]}{[GDGT - I] + [GDGT - II] + [GDGT - III] + [GDGT - 4]} \right)$$

184

185   *2.4. TOC%, CaCO$_3$% and δ^{13}C$_{org}$ analysis*

186   Total carbon (TC) and total organic carbon content (%TOC) were determined by

187   combustion of powdered samples in a Thermo Electron 1112 series Flash EA. For TOC the

188   sample was decarbonated in 10% HCl in silver capsules. %CaCO$_3$ was calculated from the

189   difference between TC and TOC. Reproducibility of %C of an internal standard was better

190   than ±0.1%. For organic carbon isotope (δ^{13}C$_{org}$) analysis samples were decarbonated in

191   10% HCl, washed to neutrality and dried. Samples were weighed into tin capsules and

192   analysed using a Flash EA connected to a ThermoFinnegan Delta V continuous flow IRMS,

193   at the Bloomsbury Environmental Isotope Facility (BEIF) at UCL. Repeat analysis of

194   internal and external standards suggests reproducibility is ±0.1‰. All stable-isotope data are

195   reported in ‰ deviation from Vienna Peedee belemnite (VPDB).

196

197   *2.5. Calcareous nannofossil analysis*

198   Calcareous nannofossil preservation and assemblage composition was determined

199   using simple smear slides and light microscopy, and observation of broken rock surfaces

200   using scanning electron microscopy (Bown and Young, 1998; Bown et al., 2008). In the

201   smear slide observations, 150 fields of view (FOV) were examined for each sample, and the

202   abundance of certain key species was determined: Abundant ("A"; >100 specimens),

203   Common ("C"; 30 – 99 specimens), Few ("F"; 9 – 29 specimens), Occasional ("O"; 3 – 8

204   specimens) or Rare ("R"; 1 – 2 specimens).

205   *2.6. Statistical analysis*

206   Simple cross-plots and linear regressions quantified with R^2 values were used to

207   ascertain the relationships between the different geochemical variables. P values to test for

208   significance were calculated on the basis of two-tailed Student's T tests. Additionally,

209   Principle Component Analysis (PCA) was carried out in SPSS 20 (Macintosh version)

210   following the methodology of Norman and Streiner (2007), on the paired samples from

211   DSDP Site 534.

212

3. Results

214   The laminated marls and the homogeneous mudstones display clear geochemical and

215   micropalaeontological differences at both Sites 534 and 603, thus supporting a different

216   depositional origin for the two lithologies (Table 1; Fig. 3; Fig. S2–S4). Importantly,

217   differences in GDGT distribution and abundance are also seen at both sites, suggesting

218   variables other than maSST influenced the TEX_{86} ratio in these early Cretaceous sediments

219   (Table 1; Fig. 3; Fig. S5). A summary of geochemical data for each site are presented in

220   Table 1, all geochemical data are plotted in Fig. 3 and are presented in full in the

221   Supplementary Information. Calcareous nannofossil data and SEM images are available in

222   the Supplementary Information (Figs. S2–S4).

9

223

224   *3.1. Lithological characterisation*

225   The laminated marls at both sites have higher $CaCO_3$ contents (averaging 70%) than

226   the homogeneous mudstones, reflecting the higher calcareous nannofossil content in this

227   lithology (Table 1; Fig. 3). The TOC distribution is more complex, but at Site 534 the

228   homogeneous mudstones generally have a higher TOC content than the corresponding

229   marls, except in certain intervals where marls have unusual organic-matter enrichment, such

230   as the mid-Valanginian (Table 1; Fig. 3).

231   The $\delta^{13}C_{org}$ data show a clear difference between lithologies, with the mudstones

232   being on average ~1.5‰ heavier than the marls at Site 534, and ~2‰ heavier at Site 603

233   (Table 1; Fig. 3). This is consistent with a higher degree of terrestrially-sourced higher plant

234   matter in the mudstones relative to the marls, coherent with the woody fragments often

235   visible in these sediments, and with earlier stable-isotope data (Dean and Arthur, 1987). The

236   abundance of terrestrial organic matter in the marls would therefore support a more neritic

237   origin for the mudstones relative to the pelagic marls. Furthermore, the mudstones at both

238   sites frequently contain pyrite framboids suggestive of reducing conditions, perhaps related

239   to the increased organic matter input and dysoxic setting of the shelf where they were

240   initially deposited, whereas the marls rarely contain any trace of pyrite (e.g., Supplementary

241   Fig. 2b).

242   While there is no systematic difference in nannofossil preservation between the two

243   lithologies, which ranges from poor to good depending on age, there are many more well-

244   preserved coccospheres and delicate taxa in the laminated marls than the homogeneous

245   mudstones, overall, particularly at Site 603 (Supplementary Fig. 2). This, combined with the

246   laminated fabric, agrees well with the notion of pelagic deposition in a quiet dysoxic

247   environment, largely free from the effects of scouring bottom currents (Robertson and

248   Bliefnick, 1983; Robertson, 1984). In agreement with previous work, the mudstones at Site

249   603 contain a higher proportion of nannoliths, such as *Nannoconus* spp*.,* and

250   *Micrantholithus* spp., compared with the corresponding marls, suggesting a neritic origin for

251   the transported mudstones, although this trend is not apparent at Site 534 where on average

252   there appears to be equal abundances of nannoliths in the mudstones and marls (Applegate

253   et al., 1989; Bornemann et al., 2008) (Figs. S3 and S4). It should be noted, however, that the

254   study interval at both Sites 534 and 603 broadly corresponds to the so called 'Valanginian

255   nannoconid decline' associated with the Weissert OAE, (Fig. 3 grey bar), which may have

256   influenced the abundance of nannoliths in the sediments at both sites (Erba et al., 2004).

257   This is supported by the fact that the separation between the mudstones and the marls, in

258   terms of nannolith abundance, does not become significant at Site 603 until after the crisis

259   ended in the mid Hauterivian (Chron M9) when the two records clearly diverge.

260   Additionally the nannoconid crisis is often reported as coinciding with a peak in *D. lehmanii*

261   abundance, which can clearly be seen at both Sites 534 and 603 (Figs. S3–S4)

262

263   *3.2. GDGT distributions*

264   Although 23 pairs of samples were analysed at Site 534, it was only possible to

265   determine the TEX_{86} values in 16 of the pairs (a ~70% success rate) as the GDGT

266   abundances were too low in the remaining samples. A similar success rate was noted for

267   samples from Site 603. However, from the available data, there is a clear difference in

268   GDGT distribution and abundance between the two lithologies at both sites, see below

269   (Table 1, Fig. 3).

270   Due to very low abundances of branched GDGTs, the BIT Index could only be

271   determined in six samples at Site 534 and four samples at Site 603, and was effectively zero

272   in the remainder of the samples. The BIT Index value for all samples, regardless of

273   lithology, was below 0.200, and generally below 0.100 (Table 1; Fig. 3), suggesting that

274   these sediments contain little or no GDGTs synthesized by soil bacteria/archaea, and

275   therefore, that the TEX_{86} values have not been unduly influenced by input of soil organic

276   matter (Hopmans et al., 2004; Weijers et al., 2006, 2010). Trends are difficult to discern as

277   the abundance of branched GDGTs was often below analytical detectability, but from the

278   sparse data available the BIT Index appears somewhat higher in the mudstones than marls of

279   similar age (Fig. 3), providing some supporting evidence for a neritic origin for the

280   mudstones. In further support of a proximal source, at Site 603 many more homogeneous

281   mudstone samples (n = 20) had detectable quantities of branched GDGTs (particularly

282   GDGTs I and II, Fig. S1) relative to the laminated marls (n = 2), and also had 16 times

283   higher average abundances of branched GDGTs (Table 1). However, as noted above, the

284   BIT Index values for the homogeneous mudstones at both Sites 534 and 603 are still very

285   low and therefore suggestive of minimal soil organic matter input, but not necessarily low

286   input of larger terrestrially-sourced debris such as wood fragments, a phenomenon which

287   has also been observed in other proximal modern settings (e.g., Huguet et al., 2007b; Walsh

288   et al., 2008). Additionally, the use of the BIT Index to track terrestrial input in ancient

289   sediments has been called into question by recent studies suggesting that fluctuations in

290   Crenarchaeol (GDGT 4) concentration, linked to marine and lacustrine productivity cycles,

291   can also drive large changes in the BIT Index (e.g., Fietz et al., 2011; Smith et al. 2012).

292   However, it is clear from the data presented in this study that the differences in BIT Index

293   values between the marls and mudstones is driven by both the abundance of the branched

294   GDGTs (which appears to be higher in the mudstones) and by the abundance of

295   Crenarchaeol (which is lower in the mudstones), at both Sites 534 and 603 (Supplementary

296   Data), and therefore is likely to reflect genuine variation in the input of terrestrially-sourced

297   GDGTs rather than merely biasing by temporal variation in marine Crenarchaeol input.

298   At site 534 the pelagic marls often contain higher normalised abundances of core

299   isoprenoid GDGTs (GDGTs 1, 2, 3, and 4') than transported mudstone samples of a similar

300   age (Table 1; Fig. 3). This is manifested in the three-fold higher average GDGT abundances

301   observed in the marls relative to the mudstones at this site (P= 0.046; Table 1). However,

302   this pattern is not evident from the Site 603 sediments, where similar average isoprenoid

303   GDGT abundances are observed in both lithologies (Table 1). There is also a persistent

304   difference in average TEX_{86}^{H} (log TEX_{86}) and TEX_{86}^{L} values between the two lithologies.

305   At Site 534, the ratios are consistently higher in the pelagic sediments (Fig. 3; Table 1), with

306   average differences between the two lithologies equating to a 0.8°C (TEX_{86}^{H} calibration) to

307   2.1°C (TEX_{86}^{L} calibration) difference in maSST estimates. The maximum difference

308   observed between the two lithologies in the same pair at Site 534 equates to a difference of

309   4°C using the $TEX_{86}L$ calibration. While these differences are small overall, the P values for

310   the two lithology populations, in terms of TEX_{86}^{H}, are <0.0001 for both sites, suggesting

311   they are significantly different (Table 1). The statistical data for the TEX_{86}^{L} values also

312   suggest a significant (P = 0.0003) difference between these two populations at Site 534.

313   Although the difference in average TEX_{86}^{H} values between marl-mudstone pairs at Site 534

314   is only above combined analytical error in three out of sixteen cases, the separation between

315   pairs is greater using the TEX_{86}^{L} calibration, being above combined error in eleven out of

316   sixteen cases (Fig. 3). Furthermore the systematic direction of offset, whereby the marls

317   nearly always yield "warmer" maSST estimates at both sites, suggest that these lithological

318   differences are not merely artifacts of random analytical error and are likely to reflect either

319   genuine SST or ecological differences between the lithologies (Fig. 3). It should be noted

320   that although lower concentrations of GDGTs have been shown to skew TEX_{86} values to

321   lower values (Schouten et al. 2007), we do not ascribe the differences between the marls and

322   the mudstones to this phenomena for three reasons: 1) the very weakest samples below a

13

323 threshold isoprenoid GDGT abundance value were excluded from consideration at both sites

324 in order to minimise possible analytical bias from very low GDGT concentrations; 2) there

325 is no significant relationship between differences in core GDGT abundances and differences

326 in TEX_{86} values between the lithologies in each pair ($R^2 = 0.2$ and 0.1 for TEX_{86}^{L} and

327 TEX_{86}^{H}, respectively; Fig. S5); 3) there is no significant difference in the normalised

328 isoprenoid GDGT abundance at Site 603 between the marls and the mudstones, despite a

329 significant difference in TEX_{86} values.

330

331 **4. Discussion**

332   The new palaeontological and geochemical data presented here (Fig. 3; Figs. S2–S4)

333 support previous observations and confirm the distinction between the autochthonous

334 pelagic laminated marls and allochthonous homogeneous mudstones (Sheridan et al., 1983;

335 Robertson and Bliefnick, 1983; Robertson, 1984; van Hinte et al., 1987; Dean and Arthur,

336 1987; Covington and Wise, 1987; Applegate et al., 1989; Bornemann et al., 2008).

337 Furthermore, systematic differences between lithologies in GDGT distribution and

338 abundance suggest a complex origin for the TEX_{86} signal in these sediments.

339   In general, the distribution of core GDGTs in sediments is thought to predominantly

340 reflect the temperature of the surface-ocean in which they were synthesized, with the flux of

341 pelagic Thaumarchaeota carried to the seafloor through biopackaging processes (e.g.,

342 Wakeham et al., 2003; Wuchter et al., 2005, 2006b). However, there are factors other than

343 maSST that can affect the core GDGT distribution in sediments and we posit three factors

344 that could explain the observed differences in core GDGT distribution between the pelagic

345 and transported facies at Sites 534 and 603:

346   (1) The different GDGT distributions record a genuine temporal or spatial difference

347 in maSST;

348   (2) Different populations or ecological preferences of Thaumarchaota in the shelf

349   and the open ocean areas produced different distributions of core GDGTs in the sediments;

350   (3) The GDGT distributions of one or both of the lithologies was influenced by

351   secondary alteration, most likely related to oxic degradation, which modified the primary

352   values.

353   Note that we can discount diagenetic thermal alteration here as downhole core GDGT

354   distributions do not change with depth and the hopane index shows no evidence for

355   overmaturation at either site (Littler et al., 2011).

356

357   *4. 1. A primary temporal or spatial difference in maSST?*

358   Although the variability in TEX_{86} indices could represent orbitally-forced climatic

359   variability within the Cretaceous greenhouse, we suggest that this is not the case. Firstly, the

360   occurrence of transported mudstones at Site 534 do not appear to display a cyclic

361   stratigraphic pattern, as might be expected if orbital forcing was influencing the redeposition

362   of the mudstone into the deep ocean. Secondly, the transported mudstones have

363   characteristics of distal turbidites (e.g., Fig. 2) and so are likely to have been deposited in a

364   geologically brief interval of time. Therefore, we assume that the closest spaced sample

365   pairs in our data represent near synchronous periods of deposition on the shelf (mudstones)

366   and in the deep-sea (hemipelagic marls). Furthermore, comparison of age-diagnostic

367   calcareous nannofossil taxa in each of the lithological pairs suggests that each was deposited

368   within the same subzone, and are therefore unlikely to differ significantly in age from one

369   another. These pairs also display a consistent direction of offset in TEX_{86} values; thereby

370   suggesting that the variability in apparent SST is not due to temporal fluctuations in climate,

371   which would perhaps be expected to display a more random pattern of change (Fig. 3).

372   Due to their distinct provenance it would not be unexpected to find different TEX$_{86}$

373   values in the mudstones and the marls, reflecting different maSSTs on the shelf and in the

374   open-ocean, as is often observed in the modern ocean (e.g., Narayan et al., 2010). The

375   "cooler" maSST values observed in the shelf-sourced mudstones, if taken at face value,

376   could be indicative of upwelled cold waters on the shelf. However, both modelling studies

377   and palaeoceanographic occurrences of organic-rich facies suggest that upwelling was more

378   likely on the eastern side of the proto-North Atlantic basin rather than in the west, where

379   Sites 534 and 603 are located, which makes this scenario less likely (Parrish and Curtis,

380   1982; Summerhayes, 1987; Handoh et al., 2003; Fig. 1). Likewise the presence of a cold

381   coastal current along the western edge of the basin cannot be ruled out on the basis of

382   present evidence, but as the dominant dirction of paleocirculation is thought to have been

383   clockwise, the western coast of the proto-North Atlantic basin would be expected to have

384   been bathed in warmer water from the lower latitudes rather than anomalously cooler waters

385   (e.g., Poulsen et al. 2001; Puceat et al., 2005). It therefore seems unlikely, but still possible,

386   that enhanced coastal upwelling or a cold current on the western side of the basin was

387   responsible for the difference in apparent maSSTs between the two lithologies, and that a

388   genuine spatial difference in SSTs is not the root cause of the variation in TEX$_{86}$ values.

389

390   *4. 2. Differences in Thaumarchaotal ecology and taxa between the shelf and the deep sea?*

391   There are several possible biological explanations for the offset in TEX$_{86}$ between

392   the pelagic and shelf sediments, including: i) spatially diverse thaumarchaeotal populations,

393   with different responses to maSST, or ii) differences in the seasonality of GDGT production

394   between the open ocean and the shelf, or iii) the influence of *in situ* sedimentary production

395   of GDGTs. These factors are difficult to deconvolve in these ancient sediments, particularly

396   in the light of the evolving understanding of modern temperate Archaea.

397   i) If taxonomically different populations of Thaumarchaeota existed in the near-

398   surface waters of the shelf and open-ocean source areas, it is possible that their response to

399   similar maSSTs, in terms of the GDGT distributions in their membranes, may have been

400   different. However, evidence for this phenomenon in the modern oceans is somewhat scant.

401   Early genetic studies of Thaumarchaeaota suggested cosmopolitan distribution in the marine

402   pelagic realm (DeLong, 1992; DeLong et al., 1994; Fuhrman et al., 1993; Massana et al.,

403   2000), but recent studies have reported more heterogeneous distributions, perhaps controlled

404   in part by the availability of ammonia (e.g., Francis et al., 2005; Agogué et al., 2008; Sintes

405   et al., 2012; Hatzenpichler, 2012; Stahl and de la Torre, 2012). In support of this

406   heterogeneity, Cao et al., (2011) found evidence of spatially-distinct archaeal populations in

407   coastal *vs*. open marine surface sediments in the western Pacific, which they suggest is

408   controlled by varying water depth and related issues such as differing nutrient supplies.

409   Furthermore, recent core-top studies documenting modern TEX_{86} values along depth-

410   transects in the South China Sea (SCS), found that while the deeper sites faithfully recorded

411   the measured average annual SSTs for that region, the shallower coastal samples

412   consistently underestimated the true annual average SST by ~2.5–9°C (Wei et al., 2011; Ge

413   et al., 2013). These spatial differences in GDGT distribution in the SCS, which are not due

414   to variations in terrestrial input as recorded by the BIT Index, are likely to be related to

415   differing Thaumarchaeaotal ecology between shallow and deeper waters. This trend, of

416   apparently "cooler" coastal sediments relative to deeper waters is similar to that observed in

417   the Cretaceous sediments in this study, but with a larger magnitude of offset.

418   ii) Although the TEX_{86} proxy is considered to be a maSST proxy, in the most recent

419   global core-top calibration TEX_{86} values were found to correlate equally well to winter

420   SSTs (R^2=0.88) and summer SSTs (R^2=0.80) as to maSSTs (R^2=0.86) (Kim et al. 2010).

421   Indeed, there is evidence to suggest that Thaumarchaeota are more abundant in the water

422   column during winter than summer, particularly in the high latitudes and within shelf seas

423   (e.g., Murray et al., 1998; Church et al., 2003; Wuchter et al., 2005, 2006a; Pitcher et al.,

424   2011). This could result in cooler than maSST TEX_{86}-based values skewed by winter

425   temperatures, as is seen in the relatively shallow, nutrient rich environment of the southern

426   North Sea, and perhaps also in the oligotrophic SCS (Herfort et al., 2006; Wei et al., 2011;

427   Ge et al., 2013). Intriguingly, this pattern of winter biased (cooler) TEX_{86} values in near-

428   shore sediments relative to the open ocean is also observed in the modern Mediterranean, a

429   basin somewhat analogous to the low-latitude, partially-restricted Cretaceous proto-North

430   Altantic (Leider et al., 2010). This seasonal skewing of temperature could therefore explain

431   the differences between Cretaceous shelf and open ocean, particularly if there was a

432   difference in nutrient content between the two regions, which fuelled periods of ammonia

433   supply and/or phytoplankton scavenging activity at different times of the year.

434   iii) Although GDGTs can be synthesised by organisms living within the sediment

435   as well as the water column (e.g., Francis et al., 2005; Biddle et al., 2006; Lipp and

436   Hinrichs, 2009), recent work suggests that the contribution of *in situ* sedimentary core

437   GDGTs production is small, due to recycling of pelagic core GDGTs in the sediment by

438   living Archaea (e.g., Takano et al., 2010; Liu et al., 2011; Bogus et al., 2012; Schouten et

439   al., 2013) and due to the relatively rapid degradation of benthic-derived intact polar lipid

440   (IPL) GDGTs within the sediment (Lengger et al., 2012). This suggests that *in situ*

441   production of GDGTs should not significantly affect TEX_{86} ratios and, therefore, cannot be

442   responsible for the differences observed in both core GDGT distribution and abundance in

443   the Cretaceous sediments. However, further work should ascertain whether any IPL-GDGTs

444   remain in the Cretaceous sediments at Sites 534 and 603, as although these molecules were

445   once thought to be quickly degraded in the marine environment (e.g., Biddle et al., 2006;

446   Huguet et al., 2010), it may be that certain types of IPL-GDGTs are more resistant to

447 degradation and so may have an influence on the TEX_{86} values of the host sediment if they

448 are at different stages of degradation (e.g., Liu et al., 2011; Lengger et al., 2012).

449

450 *4. 3. Degradation*

451   Previous studies have reported that oxic degradation has little or no systematic effect

452 on the TEX_{86} ratio in the modern marine environment (Schouten et al., 2004; Kim et al.,

453 2009b), but have also suggested that prolonged oxic degradation would reduce the total

454 abundance of core GDGTs preserved in the sediment (Schouten et al., 2004; Kim et al.,

455 2009b; Lengger et al., 2012). Data from the Plio-Pleistocene Madeira Abyssal Plane (MAP)

456 turbidite sequences suggest that oxic degradation could affect core GDGT distribution as

457 well as core GDGT abundance, but the direction of change in TEX_{86} is inconclusive

458 (Huguet et al., 2009). A study of recent Arabian Sea sediments showed differences in core

459 GDGT distribution and, consequently, TEX_{86} values between shallow organic-rich

460 sediments located in the OMZ (higher TEX_{86} values), and deeper oxic sediments with a

461 lower organic-matter content (lower TEX_{86} values), but the differences were attributed to

462 greater incorporation of deep-water GDGTs in the deeper oxic site, and not to preferential

463 preservation or degradation of specific GDGTs (Lengger et al., 2012).

464   The lack of obvious oxidation-fronts at the tops of the Cretaceous transported

465 mudstones, and the laminated nature of the pelagic sediments, suggest that the seafloor was

466 not sufficiently oxic to cause post-depositional "burn-down", as is commonly seen in recent

467 turbidites from the MAP (e.g., Wilson et al., 1986; Thomson et al., 1987). However, the

468 homogeneous mudstones, deposited in the anoxic region of the shelf and subsequently

469 transported to the dysoxic deep-sea (perhaps in a geological instant), should have

470 experienced even less oxidizing conditions (e.g., Robertson and Bleifnick, 1983; Robertson,

471 1984). Therefore, by analogy with modern evidence, we would expect a lower abundance of

472   core isoprenoid GDGTs in the dysoxic laminated marls relative to the anoxic homogeneous

473   mudstones, which is not consistent with the observed trends at Site 534, where the marls

474   have higher GDGT abundances, or at Site 603, where the two are indistinguishable (Fig. 3;

475   Table 1). It is unlikely that better preservation of core GDGTs in the carbonate-rich marls

476   can account for any difference in GDGT abundance, as fine-grained mudstones generally

477   show better preservation of organic matter than coeval carbonate-rich strata, largely due to

478   their lower porosity. Therefore, although differential degradation of core GDGTs in the

479   intercalated lithologies cannot be excluded as the cause of the TEX$_{86}$ offset, this does not

480   seem to be the most parsimonious solution, and it is instead more likely that a primary

481   difference in GDGT abundance due to differences in thaumarchaeotal ecology or taxonomy

482   is the cause of the offset.

483

484   **6. Conclusions and implications**

485   A difference in core GDGT distribution and abundance between interbedded

486   autochthonous pelagic marls and allochthonous mudstones is observed in early Cretaceous

487   sediments at North Atlantic Sites 534 and 603. Both the TEX$_{86}^{H}$ and TEX$_{86}^{L}$ ratios are

488   consistently higher in the pelagic marls than in the allochthonous mudstones, which

489   translates to an average maSST offset of ~1–2 °C, depending on calibration (Kim et al.,

490   2010). This offset may appear small, but any variation introduced by differences in host

491   lithology could be interpreted as a genuine and significant temporal maSST variation in the

492   proto-North Atlantic, when the true temporal variation in maSST may have been very low.

493   On the strength of the available evidence in these ancient sediments, it is challenging to

494   assign a definite cause for the difference in isoprenoid GDGT distribution between

495   lithologies, but it appears unlikely that the offset represents genuine temporal or spatial

496   maSST variation between the shelf and the open ocean, as the sediments are likely to be

497 coeval and no clear evidence to support enhanced coastal upwelling in the western proto-

498 North Atlantic can be found. While oxic degradation is known to influence the distribution

499 and abundance of core GDGTs in oxidised allochthonous sediments elsewhere, no evidence

500 for such oxidation is seen in the early Cretaceous sediments in this study, which have

501 characteristics of dysoxic deposition. Instead, it appears more likely that the offset reflects a

502 primary ecological difference in thaumarchaeaotal community structure, spatial distribution

503 or seasonal abundance. However, other oceanographic processes such as upwelling cannot

504 be totally discounted, and clearly more work is needed to further characterise the ecology of

505 the enigmatic Thaumarchaeota in modern settings in order to better inform the use of the

506 TEX_{86} proxy in ancient settings.

507   Importantly, it should be noted that the results of this study do not generally

508 undermine the use of the TEX_{86} palaeotemperature proxy in ancient marine settings.

509 Previous work that determined early Cretaceous maSSTs from the proto-North Altantic sites

510 reported data from the pelagic laminated marls only, and therefore the conclusions of that

511 study are not compromised by the lithological variability discussed here (Littler et al.,

512 2011). The utility of the TEX_{86} proxy for reconstructing past climates, particularly where

513 other proxies have limited range, has been successfully demonstrated in a range of studies

514 (e.g., Sluijs et al., 2006; Bijl et al., 2009), but the data from Sites 534 and 603 emphasise

515 that factors other than maSST may be influencing GDGT distributions in ancient marine

516 sediments. Therefore, careful consideration of depositional environment and history is

517 required in any palaeotemperature reconstruction using TEX_{86}.

518

519 **References**

520

521 Agogué, H., Brink, M., Dinasquet, J., Herndl, G.J., 2008. Major gradients in putatively

522   nitrifying and non-nitrifying Archaea in the deep North Atlantic. Nature 456, 788–791

523 Applegate, J.L., Bergen, J.A., Covington, J.M., Wise, S.W.J., 1989. Lower Cretaceous

524   calcareous nannofossils from continental margin drill sites off North Carolina (DSDP

525   LEG 93) and Portugal (ODP LEG 103) a comparison, in: Crux, J., Heck, S.E.V.,

526   (Eds.), Nannofossils and Their Applications. Ellis Horwood, Chichester, pp. 212–222

527 Biddle, J. F., Lipp, J.S., Lever, M.A., Lloyd, K.G., Sørensen, K.B., Anderson, R.D.,

528   Fredricks, H.F., Elvert, M., Kelly, T.J., Schrag, D.P., Sogin, M.L., Brenchley, J.E.,

529   Teske, A., House, C.H., Hinrichs, K–U., 2006. Heterotrophic Archaea dominate

530   sedimentary subsurface ecosystems off Peru. Proceedings of the National Academy of

531   Science 103, 3846–3851

532 Bijl, P.K., Schouten, S., Sluijs, A., Reichart, G-J., Zachos, J.C., Brinkhuis, H., 2009. Early

533   Palaeogene temperature evolution of the southwest Pacific Ocean. Nature 461, 776–

534   779

535 Bogus, K.A., Zonneveld, K.A.F., Fischer, D., Kasten, S., Bohrmann, G., Versteegh. G.J. M.,

536   2012. The effect of meter-scale lateral oxygen gradients at the sediment-water

537   interface on selected organic matter based alteration, productivity and temperature

538   proxies. Biogeosciences 9, 1553–1570. doi:10.5194/bg-9-1553-2012

539 Bornemann, A., Mutterlose, J., 2008. Calcareous nannofossil and $\delta^{13}C$ records from the

540   Early Cretaceous of the western Atlantic Ocean: evidence for enhanced fertilization

541   across the Berriasian–Valanginian transition. Palaios 23, 821–832

542 Bown, P.R., Young, J.R., 1998. Techniques, in: Bown P.R (Ed.), Calcareous Nannofossil

543   Biostratigraphy. Kluwer Academic Publishers, London, pp. 16–28

544 Bown, P.R., Dunkley Jones, T., Lees, J.A., Pearson, P.N., Young, J.R., Randell, R., Coxall,

545   H.K., Mizzi, J., Nicholas, C.J., Karega, A., Singano, J., Wade, B.S., 2008. A

546   Paleogene calcareous microfossil Konservat-Lagerstatte from the Kilwa Group of

547   coastal Tanzania. Geological Society of America Bulletin 120, 3–12

548   Brochier-Armanet, C., Boussau, B., Gribaldo, S., Forterre, P., 2008. Mesophilic

549   crenarchaeota: Proposal for a third archaeal phylum, the Thaumarchaeota. Nature

550   Reviews Microbiology 6, 245–252

551   Cao, H., Hong, Y., Li, M., Gu, J-D., 2011. Phylogenetic Diversity and Ecological Pattern of

552   Ammonia-oxidizing Archaea in the Surface Sediments of the Western Pacific.

553   Microbial Ecology 62, 813–823

554   Church, M. J., DeLong, E.F., Ducklow, H.W., Karner, M.B., Preston, C.M., Karl, D.M.,

555   2003. Abundance and distribution of planktonic *Archaea* and *Bacteria* in the Western

556   Antarctic Peninisula. Limnology and Oceanography 48, 1893–1902

557   Covington, J.M., Wise, S.W., Jr., 1987. Calcareous nannofossil biostratigraphy of a lower

558   Cretaceous deep–sea fan complex: Deep Sea Drilling Project Leg 93 Site 603, lower

559   continental rise off Cape Hatteras, in: van Hinte, J. E., Wise, S. W., Jr., et al., Initial

560   Reports of the Deep Sea Drilling Project 93, Washington (U.S. Govt. Printing Office),

561   pp. 617–660

562   Dean, W.E., Arthur, M.A., 1987. Inorganic and organic geochemistry of Eocene to

563   Cretaceous Strata recovered from the Lower Continental Rise, North American Basin,

564   Site 603, Deep Sea Drilling Project Leg 93, in: van Hinte, J. E., Wise, S. W., Jr., et al.,

565   Initial Reports of the Deep Sea Drilling Project 93, Washington (U.S. Govt. Printing

566   Office), pp. 1093–1137

567   Dean, W.E., Arthur, M.A., 1999. Sensitivity of the North Atlantic basin to cyclic climatic

568   forcing during the Early Cretaceous. Journal of Foraminiferal Research 29(4), 465–

569   486

570   DeLong, E.F., 1992. Archaea in coastal marine environments. Proceedings of the National

571   Academy of Sciences 89, 5685−5689

572   Dunham, K.W., Meyers, P.A., Dunham, P.L., 1987. Organic geochemical comparison of

573   Cretaceous black shales and adjacent strata from deep sea drilling project Site 603,

574   Outer Hatteras Rise, in: van Hinte, J. E., Wise, S. W., Jr., et al., Initial Reports of the

575   Deep Sea Drilling Project 93, Washington (U.S. Govt. Printing Office), pp. 25–226

576   Erba, E., Bartolini, A., Larson, R.L., 2004. Valanginian Weissert oceanic anoxic event

577   Geology 32, 149–152. doi: 10.1130/G20008.1

578   Fietz, S., Martínez-Garcia, A., Huguet, C., Rueda, G., Rosell-Melé, A., 2011. Constraints in

579   the application of the Branched and Isoprenoid Tetraether index as a terrestrial input

580   proxy. Journal of Geophysical Research: Oceans 116, doi: 10.1029/2011JC007062

581   Francis, C.A., Roberts, K.J., Berman, J.M., Santoro, A.E., Oakley, B.B., 2005. Ubiquity and

582   diversity of ammonia–oxidising archaea in water columns and sediments of the ocean.

583   Proceedings of the National Academy of Sciences 102, 14683–14688

584   Frank, T.D., Arthur, M.A., Dean, W.E., 1999. Diagenesis of Lower Cretaceous pelagic

585   carbonates, North Atlantic: paleoceanographic signals obscured. Journal of

586   Foraminiferal Research 29(4), 340–351

587   Fuhrman, J.A., McCallum, K., Davis, A.A., 1993. Phylogenetic diversity of subsurface

588   marine microbial communities from the Atlantic and Pacific oceans. Applied and

589   Environmental Microbiology 59, 1294–1302

590   Ge, H., Zhang C.L., Dang, H., Zhu, C., Jia, G., 2013. Distribution of tetraether lipids in

591   surface sediments of the northern South China Sea: Implications for TEX_{86} proxies.

592   Geoscience Frontiers 4, 223–229

593   Handoh, I.C., Bigg, G.R., Jones, E.J.W., 2003. Evolution of upwelling in the Atlantic Ocean

594   basin. Palaeogeography, Palaeoclimatology, Palaeoecology 202, 31–58

595   Hatzenpichler, R., 2012. Diversity, Physiology and niche differentiation of ammonia-

596   oxidizing archaea. Applied Environmental Microbiology 78(21), 7501. doi:

597   10.1128/AEM.01960-12

598   Herbin, J.P., Deroo, G., Roucaché, J., 1983. Organic Geochemistry in the Mesozoic and

599   Cenozoic Formations of Site 534, Leg 76, Blake-Bahama Basin, and Comparison with

600   Site 391, Leg 44. Initial reports of the Deep Sea Drilling Project 76, 481–493

601   Herfort, L., Schouten, S., Boon, J.P., Sinninghe Damsté, J.S., 2006. Application of the

602   TEX_{86} temperature proxy to the southern North Sea. Organic Geochemistry 37, 1715–

603   1726

604   Hollis, C.J., Taylor, K.W.R., Handley, L., Pancost, R.D., Huber, M., Creech, J.B., Hines,

605   B.R., Crouch, E.M., 2012. Early Paleogene temperature history of the Southwest

606   Pacific Ocean: Reconciling proxies and models. Earth Planet Sci. Lett. 349–350, 53–

607   66

608   Hopmans, E.C., Weijers, J.W.C, Schefuß, E., Herfort, L., Sinninghe Damsté, J.S., Schouten,

609   S., 2004. A novel proxy for terrestrial organic matter in sediments based on branched

610   and isoprenoid tetraether lipids, Earth and Planetary Science Letters 224, 107–116

611   Huguet, C., Schimmelmann, A., Thunell, R., Lourens, L.J., Sinninghe Damsté, J.S.,

612   Schouten, S., 2007a. A study of the TEX_{86} paleothermometer in the water column and

613   sediments of the Santa Barbara Basin, California. Paleoceanography 22, PA3203

614   Huguet, C., Smittenberg, R., Boer, W., Sinninghe Damsté, J.S., Schouten, S., 2007b.

615   Twentieth century proxy records of temperature and soil organic matter input in the

616   Drammensfjord, southern Norway. Organic Geochemistry 38, 1838–1849

617   Huguet, C., Kim, J–H., de Lange, G–J., Sinninghe Damsté, J.S., Schouten, S., 2009. Effects

618   of long term oxic degradation on the UK^{37}, TEX_{86} and BIT organic proxies. Organic

619   Geochemistry 40, 1188–1194

620   Huguet, C., Urakawa, H., Martens-Habbena, W., Truxal, L., Stahl, D.A., Ingalls, A.E.,

621   2010. Changes in intact membrane lipid content of archaeal cells as an indication of

622   metabolic status. Organic Geochemistry 41, 930–934

623   Hsü, K. J., Jenkyns, H.C., 1974. Editors, Pelagic sediments: on land and under the sea.

624   Special Publication of the International Asscociation of Sedimentologists 1, 1–10.

625   Blackwell Scientific Publications. doi: 10.1002/9781444304855

626   Ingalls, A.E., Shah, S.R., Hansman, R.L. Aluwihare, L.I., Santos, G.M., Druffel E.R.M.,

627   Pearson, A., 2006. Quantifying archaeal community autotrophy in the mesopelagic

628   ocean using natural radiocarbon. Proceedings of the National Accademy of Sciences

629   103, 6442–6447

630   Jenkyns, H.C., Schouten-Huibers, L., Schouten, S., Sinninghe Damsté, J.S., 2012. Warm

631   Middle Jurassic–Early Cretaceous high-latitude sea-surface temperatures from the

632   Southern Ocean. Climate of the Past 8, 215–226

633   Karner, M.B., DeLong, E.F., Karl, D.M., 2001. Archaeal dominance in the mesopelagic

634   zone of the Pacific Ocean. Nature 409, 507–510

635   Katz, B.J., 1983. Organic geochemical character of some Deep Sea Drilling Project cores

636   from Legs 76 and 44. Initial reports of the Deep Sea Drilling Project 76, in: Sheridan,

637   R.E., Gradstein, F.M., et al., Initial Reports of the Deep Sea Drilling Project 76,

638   Washington (U.S. Govt. Printing Office), pp. 463–468

639   Kim, J–H., Schouten, S., Hopmans, E.C., Donner, B., Sinninghe Damsté, J.S., 2008. Global

640   sediment core–top calibration of the TEX_{86} paleothermometer in the ocean.

641   Geochimica et Cosmochimica Acta 72, 1154–1173

642   Kim, J–H, Crosta, X., Michel, E., Schouten, S., Duprat, J., Sinninghe Damsté, J.S., 2009a.

643   Impact of lateral transport on organic proxies in the Southern Ocean. Quaternary

644   Research 71, 246–250, doi: 10.1016/j.yqres.2008.10.005

645   Kim, J–H., Huguet, C., Zonneveld, K.A.F., Versteegh, G.J.M., Roeder, W., Sinninghe

646   Damsté, J.S., Schouten, S., 2009b. An experimental field study to test the stability of

647   lipids used for the TEX_{86} and U^K_{37} palaeothermometers. Geochimica et

648   Cosmochimica Acta 73, 2888–2898

649   Kim, J–H., van der Meer, J., Schouten, S., Helmke, P., Willmott, V., Sangiorgi, F., Koc, N.,

650   Hopmans, E.C., Sinninghe Damsté, J.S., 2010. New indices and calibrations derived

651   from the distribution of crenarchaeal isoprenoid tetraether lipids: Implications for past

652   sea surface temperature reconstructions. Geochimica et Cosmochimica Acta 74, 4639–

653   4654

654   Könneke, M., Bernhard, A.E., de la Torre, J.R., Walker, C.B., Waterbury, J.B., Stahl, D.A.,

655   2005. Isolation of an autotrophic ammonia–oxidizing marine archaeon. Nature 437,

656   543–546

657   Leider, A., Hinrichs, K-U., Mollenhauer, G., Versteegha, G.J.M., 2010. Core-top calibration

658   of the lipid-based UK37 and TEX86 temperature proxies on the southern Italian shelf

659   (SW Adriatic Sea, Gulf of Taranto). Earth and Planetary Science Letters 300, 112–124

660   Lengger, S.K., Hopmans, E.C., Reichart, G-J., Nierop, K.G.J., Sinninghe Damsté, J.S.,

661   Schouten, S., 2012. Intact polar and core glycerol dibiphytanyl glycerol tetraether

662   lipids in the Arabian Sea oxygen minimum zone. Part II: Selective preservation and

663   degradation in sediments and consequences for the TEX_{86}. Geochimica et

664   Cosmochimica Acta 98, 244–258

665   Lipp, J.S., Hinrichs, K–U., 2009. Structural diversity and fate of intact polar lipids in marine

666   sediments. Geochimica et Cosmochimica Acta 73, 6816–6833

667   Littler, K., Robinson, S.A., Bown, P.R., Nederbragt, A.J., Pancost, R.D., 2011. High sea-

668   surface temperatures during the Early Cretaceous Epoch. Nature Geoscience 4, 169–

669   172

670 Liu, X.L., Lipp, J.S., Hinrichs K-U., 2011. Distribution of intact and core GDGTs in marine

671   sediments. Organic Geochemistry 42, 368–375

672 Massana, R., DeLong, E.F., Pedros–Alio, C., 2000. A few cosmopolitan phylotypes

673   dominate planktonic archaeal assemblages in widely different oceanic provinces.

674   Applied Environmental Microbiology 66, 1777–1787

675 Martens-Habbena, W., Berube, P.M., Urakawa, H., de la Torre, J.R., Stahl, D.A., 2009.

676   Ammonia oxidation kinetics determine niche separation of nitrifying Archaea and

677   Bacteria. Nature 461, 976–981

678 Menzel, D., Hopmans, E.C., Schouten, S., Sinninghe Damsté, J.S., 2006. Membrane

679   tetraether lipids of planktonic Thaumarchaeota in Pliocene sapropels of the eastern

680   Mediterranean Sea. Palaeogeography, Palaeoclimatology, Palaeoecology 239, 1–15

681 Mincer, T.J., Church, M.J., Trent, Taylor, L., Preston, C., Karl, D.M., DeLong, E.F., 2007.

682   Quantitative distribution of presumptive archaeal and bacterial nitrifiers in Monterey

683   Bay and the North Pacific Subtropical Gyre. Applied Environmental Microbiology 9,

684   1162–1175

685 Mollenhauer, G., Inthorn, M., Vogt, T., Zabel, M., Sinninghe Damsté, J.S., Eglinton, T.I.,

686   2007. Aging of marine organic matter during cross-shelf lateral transport in the

687   Benguela upwelling system revealed by compound-specific radiocarbon dating.

688   Geochemistry Geophysics, Geosystems 8. Q09004

689 Mollenhauer, G., Eglinton, T.I., Hopmans, E.C., Sinninghe Damsté, J.S., 2008. A

690   radiocarbon-based assessment of the preservation characteristics of crenarcheol and

691   alkenones from continental margin sediments. Organic Geochemistry 39, 1039–1045

692 Narayan, N., Paul, A., Mulitza, S., Schulz, M., 2010. Trends in coastal upwelling intensity

693   during the late 20th century. Ocean Sciences 6, 815–823

694   Norman, G.R., Streiner, D.L., 2007. Principal Components and Factor Analysis, in:

695   Norman, G.R., Streiner, D.L. (Eds.), Biostatistics: The Bare Essentials. PMPH-USA,

696   pp 194–209

697   Ocean Drilling Stratigraphic Network (ODNS), Plate Tectonic Reconstruction Service

698   Paleomap project (http://www.odsn.de/odsn/services/paleomap/paleomap.html)

699   (2013)

700   Ogg, J.G., 1987. Early Cretaceous magnetic polarity time scale and the magnetostratigraphy

701   of deep sea drilling project sites 603 and 534, western central Atlantic, in: van Hinte,

702   J. E., Wise, S. W., Jr., et al., Initial Reports of the Deep Sea Drilling Project 93,

703   Washington (U.S. Govt. Printing Office), pp. 849–880

704   Ouverney, C.C., Fuhrman, J.A., 2000. Marine planktonic Archaea take up amino acids.

705   Applied and Environmental Microbiology 66, 4829–4833

706   Parrish, J.T., Curtis, R.L., 1982. Atmospheric circulation, upwelling, and organic-rich rocks

707   in the Mesozoic and Cenozoic eras. Palaeogeography, Palaeoclimatology,

708   Palaeoecology 40, 31–66

709   Pearson, A., McNichol, A.P., Benitez–Nelson, B.C., Hayes, J.M., Eglinton, T.I., 2001.

710   Origins of lipid biomarkers in Santa Monica Basin surface sediment: A case study

711   using compound–specific d^{14}C analysis. Geochimica et Cosmochimica Acta 65,

712   3123–3137

713   Pitcher, A.E., Wuchter, C., Siedenberg, K., Schouten, S., Sinninghe Damsté, J.S., 2011.

714   Crenarchaeol tracks winter blooms of ammonia-oxidizing Thaumarchaeota in the

715   coastal North Sea. Limnology and Oceanography 56, 2308–2318

716   Poulsen, C.J., Barron, E.J., Arthur, M.A., Peterson, W.H., 2001. Response of the mid-

717   Cretaceous global oceanic circulation to tectonic and CO_2 forcing. Paleoceanography

718   16, 576– 592

719   Pucéat, E., Lécuyer, C., Reisberg, L., 2005. Neodymium isotope evolution of NW Tethyan

720   upper ocean waters throughout the Cretaceous. Earth and Planetary Science Letters

721   236, 705– 720

722   Robertson, A.H.F., Bliefnick, D.M., 1983. Sedimentology and origin of Lower Cretaceous

723   pelagic carbonates and deposited clastics, Blake–Bahama formation, Deep Sea

724   Drilling Project Site 534, Western Equatorial Atlantic, in: Sheridan, R.E., Gradstein,

725   F.M., et al., Initial Reports of the Deep Sea Drilling Project 76, Washington (U.S.

726   Govt. Printing Office), pp., 795–828

727   Robertson, A.H.F., 1984. Origin of varve-type lamination, graded claystones and limestone-

728   shale 'couplets' in the lower Cretaceous of the western North Atlantic. Geological

729   Society of London, Special Publications 15, 437–452

730   Schouten, S., Hopmans, E.C., Schefuß, E., Sinninghe Damsté, J.S., 2002. Distributional

731   variations in marine crenarchaeotal membrane lipids: a new tool for reconstructing

732   ancient sea water temperatures? Earth and Planetary Science Letters 204, 265–274

733   Schouten, S., Hopmans, E.C., Sinninghe Damsté, J.S., 2004. The effect of maturity and

734   depositional redox conditions on archaeal tetraether lipid palaeothermometry. Organic

735   Geochemistry 35, 567–571, doi: 10.1016/j.orggeochem.2004.01.012

736   Schouten, S., Huguet, C., Hopmans, E.C., Kienhuis, M.V.M., Sinninghe Damsté, J.S., 2007.

737   Analytical methodology for TEX_{86} paleothermometry by High–Performance Liquid

738   Chromatography/Atmospheric Pressure Chemical Ionization–Mass Spectrometry.

739   Analytical Chemistry 79, 2940–2944

740   Schouten, S., Hopmans, E.C., Sinninghe Damsté, J.S., 2013. The organic geochemistry of

741   glycerol dialkyl glycerol tetraether lipids: A review. Organic Geochemistry 54, 19–61

742   Shah, S.R., Mollenhauer, G., Ohkouchi, N., Eglinton, T.I., Pearson, A., 2008. Origins of

743   archaeal tetraether lipids in sediments: Insights from radiocarbon analysis.

744   Geochimica et Cosmochimica Acta 72, 4577–4594

745   Sheridan, R.E., Gradstein, F.M., et al., 1983. Site 534. Initial Reports of the Deep Sea

746   Drilling Project 76, Washington (U.S. Govt. Printing Office), pp. 141–340

747   Sinninghe Damsté, J.S., Rijpstra, W.I.C., Reichart, G., 2002. The influence of oxic

748   degradation on the sedimentary biomarker record II. Evidence from Arabian Sea

749   sediments. Geochimica et Cosmochimica Acta 66, 2737–2754

750   Sluijs, A., Schouten, S., Pagani, M., Woltering, M., Brinkhuis, H., Sinninghe Damsté, J.S.,

751   Dickens, G.R., Huber, M., Reichart, G-J., Stein, R., Matthiessen, J., Lourens, L.J.,

752   Pedentchouk, N., Backman, J., Moran, K., and the Expedition 302 Scientists 2006.

753   Subtropical Arctic Ocean temperatures during the Palaeocene/Eocene thermal

754   maximum. Nature 441, 610–613

755   Smith, R.W., Bianchi, T.S., Li, X., 2012. A re-evaluation of the use of branched GDGTs as

756   terrestrial biomarkers: Implications for the BIT Index. Geochimica et Cosmochimica

757   Acta 80, 14–29.

758   Stahl, D.A., de la Torre, J.R., 2012. Physiology and Diversity of Ammonia-Oxidizing

759   Archaea. Annual Review of Microbiology 66, 83–101. doi: 10.1146/annurev-micro-

760   092611-150128

761   Summerhayes, C.P., 1987. Organic-rich Cretaceous sediments from the North Atlantic.

762   Geological Society of London, Special Publications 26, 301–316

763   Taylor, K.W.R., Huber, M., Hollis, C.J., Hernandez-Sanchez, M.T., Pancost, R.D., 2013.

764   Re-evaluating modern and Palaeogene GDGT distributions: Implications for SST

765   reconstructions. Global and Planetary Change 108, 158–174

766   Thomson, J., Colley, S., Higgs, N.C., Hydes, D.J., Wilson, T.R.S., 1987. Geochemical

767   oxidation fronts in NE Atlantic distal turbidites and their effects in the sedimentary

768   record. Geological Society of London, Special Publications 31, 167–177

769   van Hinte, J.E., Wise, S.W., Jr., et al., 1987. Site 603. Initial Reports of the Deep Sea

770   Drilling Project 93, Washington (U.S. Govt. Printing Office), pp. 25–226

771   Wakeham, S.G., Lewis, C.A., Hopmans, E.C., Schouten, S., Sinninghe Damsté, J.S., 2003.

772   Archaea mediate anaerobic oxidation of methane in deep euxinic waters of the Black

773   Sea. Geochimica et Cosmochimica Acta 67, 1359–1374

774   Walsh, E.M., Ingalls, A.E., Keil, R.G., 2008. Sources and transport of terrestrial organic

775   matter in Vancouver Island fjords and the Vancouver–Washington Margin: A

776   multiproxy approach using δ^{13}Corg, lignin phenols, and the ether lipid BIT index.

777   Limnology and Oceanography 53, 1054–1063

778   Wei, Y., Wang, J., Liu, J., Dong, L., Li, L., Wang, H., Wang, P., Zhao, M., Zhang, C.L.,

779   2011. Spatial variations in archeal lipids of surface water and core-top sediments in

780   the South China Sea and their implications for paleoclimate studies. Applied and

781   Environmental Microbiology 77 (21), 7479–7489

782   Weijers, J.W.H., Schouten, S., Spaargaren, O.C., Sinninghe Damsté, J.S., 2006. Occurrence

783   and distribution of tetraether membrane lipids in soils: Implications for the use of the

784   TEX$_{86}$ proxy and the BIT index. Organic Geochemistry 37, 1680–1693

785   Weijers, J.W.H., Wiesenberg, G.L.B., Bol, R., Hopmans, E.C., Pancost, R.D., 2010. Carbon

786   isotopic composition of branched tetraether membrane lipids in soils suggest a rapid

787   turnover and a heterotrophic life style of their source organism(s). Biogeosciences 7,

788   2959–2973

789   Weijers, J.W.H., Lim, K.L.H., Aquilina, A., Sinninghe Damsté, J.S., Pancost, R.D., 2011.

790   Biogeochemical controls on glycerol dialkyl glycerol tetraether lipid distributions in

791   sediments characterized by diffusive methane flux. Geochemistry, Geophysics,

792   Geosystems 12, Q10010, 15

793   Wilson, T.R.S., Thomson, J., Hydes, D.J., Colley, S., Culkin, F., Sørensen, J., 1986.

794   Oxidation Fronts in Pelagic Sediments: Diagenetic Formation of Metal-Rich Layers.

795   Science 232, 972–975

796   Wuchter, C., Schouten, S., Wakeham, S.G., Sinninghe Damsté, J.S., 2005. Temporal and

797   spatial variation in tetraether membrane lipids of marine Crenarchaeota in particulate

798   organic matter: Implications for TEX_{86} paleothermometry. Paleoceanography 20,

799   PA3013

800   Wuchter, C., Abbas, B., Coolen, M.J.L., Herfort, L., van Bleijswijk, J., Timmers, P., Strous,

801   M., Teira, E., Herndl, G.J., Middelburg, J.J., Schouten, S., Sinninghe Damsté, J.S.,

802   2006a. Archaeal nitrification in the ocean. Proceedings of the National Academy of

803   Science 103, 12317–12322

804   Wuchter, C., Schouten, S., Wakeham, S.G., Sinninghe Damsté, J.S., 2006b. Archaeal

805   tetraether membrane lipid fluxes in the northeastern Pacific and the Arabian Sea:

806   implications for TEX_{86} paleothermometry. Paleoceanography 21, PA4208

807

808   Acknowledgements

809

Figure Captions

Fig. 1. Reconstructed palaeogeography of the proto-North Atlantic region in the Early Hauterivian (~133 Ma). Location of DSDP Sites 534 and 603 shown as black circles; likely surface circulation pattern shown as grey arrows after Puceat et al., (2005) and Poulsen et al. (2001), with area of probable upwelling (hatched area) after Parrish and Curtis (1982) and Handoh et al., (2003). Palaeogeography adapted form the Ocean Drilling Stratigraphic Network plate tectonic reconstruction service (http://www.odsn.de/odsn/services/paleomap/paleomap.html).

Fig. 2. A representative core section from DSDP 76-534A-64-02, 110–122 cm. DLM = Dark coloured Laminated Marl; LLM = Light coloured Laminated Marl; HM = Homogeneous mudstone; SS = Sandstone; BC = Bioturbated Chalk. Although obscured by fragmentation of the core, sharp boundaries between the base of the homogeneous mudstones and the top of the laminated marls can be seen, with a more gradational boundary between the top of the mudstones and the base of the marls.

Fig. 3. Geochemical data from a) DSDP Site 534 and b) DSDP Site 603. Error bars on the TEX_{86}^{H} and TEX_{86}^{L} data represent the analytical error (±0.012; 1σ). Calibration error when converting to maSST is ±4 °C for TEX_{86}^{L} and ±2.5 °C for TEX_{86}^{H} (Kim et al., 2010). GDGT = the abundance of isoprenoid GDGTs (1, 2, 3 and 4'), normalised per gram of dry bulk sediment and per μl of solvent injected onto the LC column, normalised to the isoprenoid GDGT abundance of the internal standard for that analysis. Grey bar in *Nannoconus spp*. box represents approximate duration of the 'nannoconid crisis', after Erba et al., 2004.

Table 1. Summary of averaged geochemical results from a) DSDP Site 534, b) DSDP Site 603. n = the number of analyses in each category, as not all samples yielded data for each geochemical parameter. Iso-GDGT = isoprenoid GDGT abundances (GDGTs 1, 2, 3 and 4'), normalised per gram of bulk sediment extracted and per μl of solvent injected on the LC column, normalised to the isoprenoid GDGT abundance of the internal standard for that analysis. Br-GDGT = Branched GDGT abundance, scaled in the same way as the isoprenoid GDGTs. Note that the abundance of Br-GDGTs in many of the samples was '0', hence the average abundance values here will not be representative of the mean of the successful samples. Note the n = values listed under Br-GDGT represent the number of samples containing any branched GDGTs, not the number of samples for which there were sufficient samples to construct a BIT Index. P values are for unpaired, two-tailed Student's T-tests.

Supplementary Figure Captions

Fig. S1. The structure and nomenclature of the isoprenoid and branched core GDGT molecules discussed in this paper.

Fig. S2a. Scanning electron micrographs of rock surfaces from paired marl and mudstone samples (**ABCD**). **A and B** = DSDP 534A-60-04, 63cm; homogeneous mudstone. **A** = X 7,500 mag. Clayrich containing well-preserved coccoliths. A *Cretarhabdus madingleyensis* is indicated by a yellow arrow, showing fine central structures, and a somewhat etched *Axopodorhabdus dietzmanii* is indicated by green

arrow. **B** = X 7000 mag. Clay flakes and a *Nannoconus* sp. **C and D** = DSDP 534A-60-04, 66cm; laminated marl. **C** = X 8,000 mag. Well preserved coccoliths and clay flakes. *Lithraphidites carniolensis* is common throughout (purple arrow) and *Rotelapillus laffittei* (pale blue arrow) is quite common and shows good preservation of the delicate central bars. **D** = X 8,000 mag. *Watznaueria barnesiae* coccosphere. Some secondary calcite is visible, but coccoliths are generally well-preserved. **E and F** = DSDP 534A-69-05, 34 cm; laminated marl. **E** = X 5,500 mag. Well-preserved *Watznaueria* sp. coccosphere, surrounded by *W. barnesiae* and *Diazomatolithus lehmanii* fragments. *Cretarhabdus conicus* visible in bottom left (red arrow), and small *Zeugrhabdotus* spp. (green arrow) to the left. **F** = X 6,000 mag. Well-preserved coccoliths including *Axopodorhabdus dietzmanii* (yellow arrow), with *D. lehmanii*, (red arrows), with *W. barnesiae* (blue arrows), *Stradnerlithus geometricus* (purple arrows) and two different *Zeugrhabdotus* spp. (green arrows).

Fig. S2b. Scanning electron micrographs of rock surfaces from sample DSDP 603B-57-05, 49 cm (**ABCD**); laminated marl, excellent preservation. **A** = X 4,300 mag. Dominated by very well-preserved calcareous nannofossils, including *W. barnesiae* (yellow arrows), *D. lehmanii* (red arrows), *Zeugrhabdotus* spp. (green arrow), *R. laffittei* (purple arrow), *Stradnerlithus asymmetricus* (blue arrow). **B** = X 16,000 mag. *Cretarhabdus inaequalis* showing well-preserved central grill structure. **C** = X 4,300 mag. Well-preserved *Stradnerlithus asymmetricus* (blue arrow) surrounded by *Biscutum constans* (yellow arrow) and *D. lehmanii* (red arrow). **D** = X 13,000 mag. Well-preserved *Helenea chiastia*. **E and F** = DSDP 603B-75-03, 85 cm; homogeneous mudstone. **E** = X 1,500 mag. A cluster of pyrite framboids surrounded by clay flakes. **F** = X 2,700 mag. Clay containing moderately preserved calcareous

nannofossils, including *D. lehmanii* (red arrows) and a small *Zeugrhabdotus* spp. (green arrow).

Fig. S3. Calcareous nannofossil data from DSDP Site 534, showing abundance data from selected species and genera only. Grey bar indicates approximate span of the 'nannoconid crisis' after Erba et al., 2004, which is also associated with a peak in *D. lehmanii* in Tethyan sections.

Fig. S4. Calcareous nannofossil data from DSDP Site 603, showing abundance data from selected species and genera only. Grey bar indicates approximate span of the 'nannoconid crisis' after Erba et al., 2004, which is also associated with a peak in *D. lehmanii* in Tethyan sections.

Fig. S5. a) Cross-plots for data from DSDP Site 534. The difference (Δ) between each individual lithology pair (a mudstone and a marl from a similar depth in the core), in terms of TEX_{86} ratios and isoprenoid GDGT concentrations (normalised to 1 g of dry bulk sediment and 1 μl of solvent injected onto the LC column, and to the GDGT abundance of the internal standard), are cross-plotted to show the lack of relationship; i.e., the difference in GDGT concentration between the mudstone and the marls is not causing the offset in TEX_{86} values, regardless of calibration. Simple linear regressions are shown and quantified with R^2 values. **b)** PCA analysis carried out in SPSS. Scree plot and component plot for the 9 variables that characterize the Site 534 samples (difference between marls and mudstones in terms of: depth, TEX_{86}, TEX_{86}^{L}, TEX_{86}^{H}, GDGT abundance, GDGT-2 / GDGT-3 ratio, %TOC, %CaCO_3, and $\delta^{13}C$). The Kaiser-Meyer-Olkin Measure of Sampling Adequacy is below the 0.6 threshold,

suggesting this dataset does not pass the basic assumptions required for PCA analysis. Additionally, no principle components could be identified at the rotated component matrix stage, and no clustering is obvious from the component plot, suggesting no strong underlying relationship between the various geochemical variables.

XLS file:

Supplementary Data**.** All geochemical data including raw isoprenoid and branched GDGT abundances.

Fig. 1.
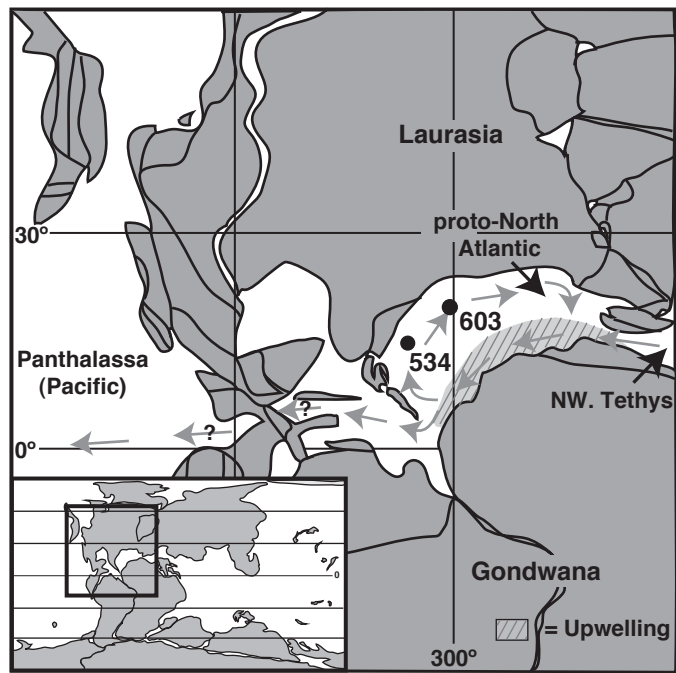
Fig. 2.

Fig. 3.

a) DSDP Site 534

b) DSDP Site 603

Nannoconus spp. | *Micranthrolithus spp.* | CaCO$_3$% | TOC% | δ^{13}C$_{org}$ (VPDB) | TEX$_{86}$-L | TEX$_{86}$-H | Isoprenoid GDGT | BIT Index
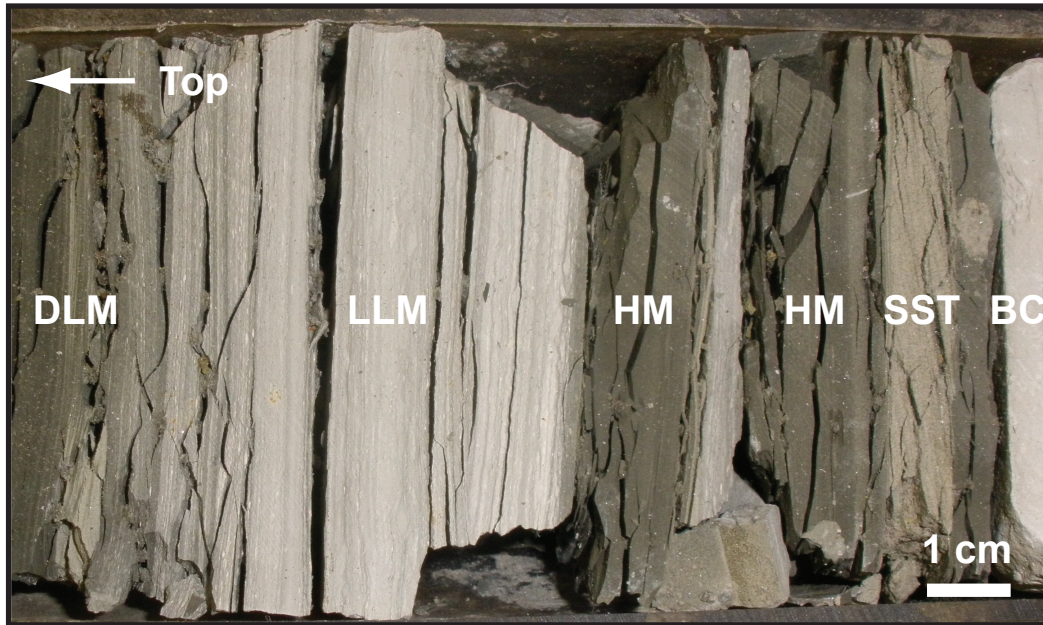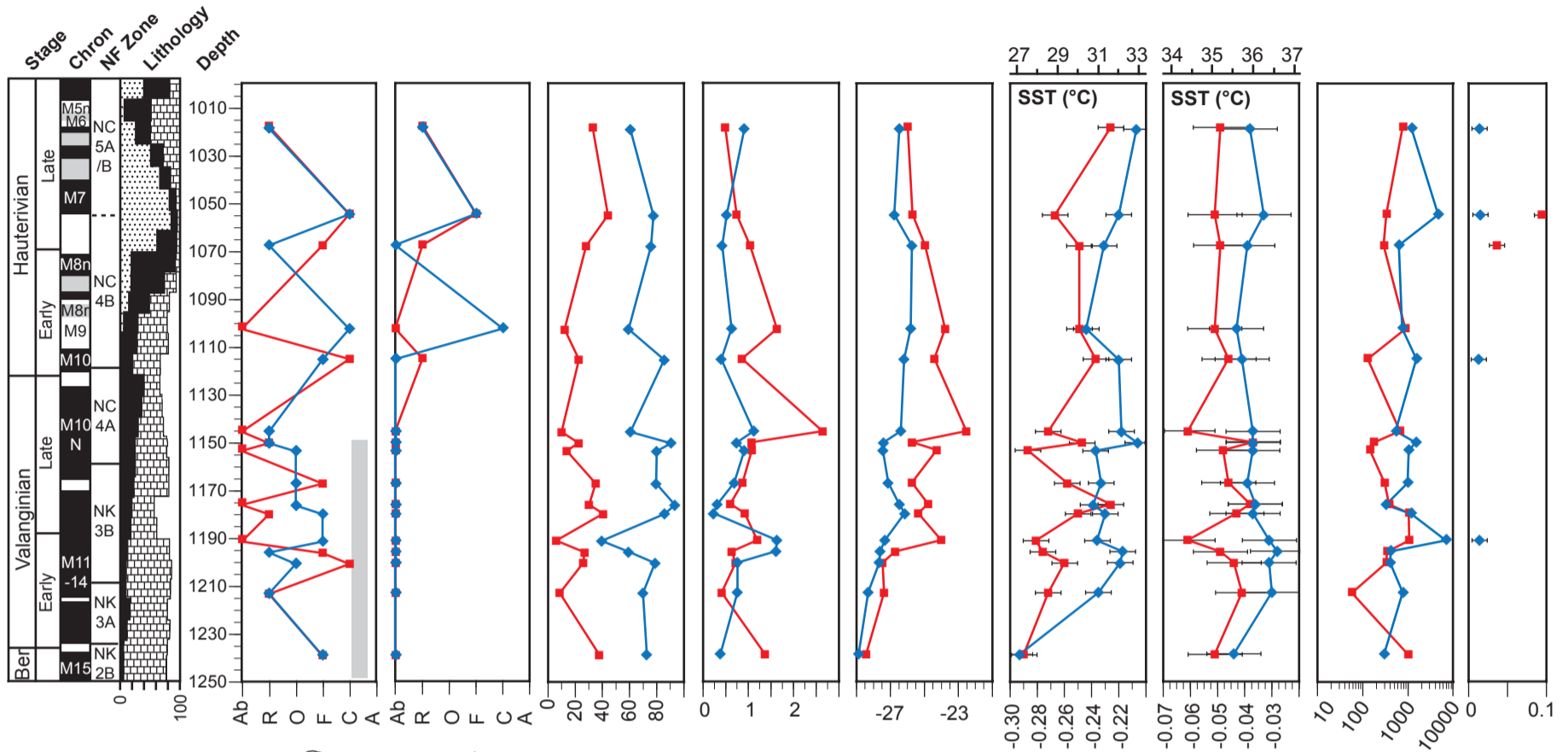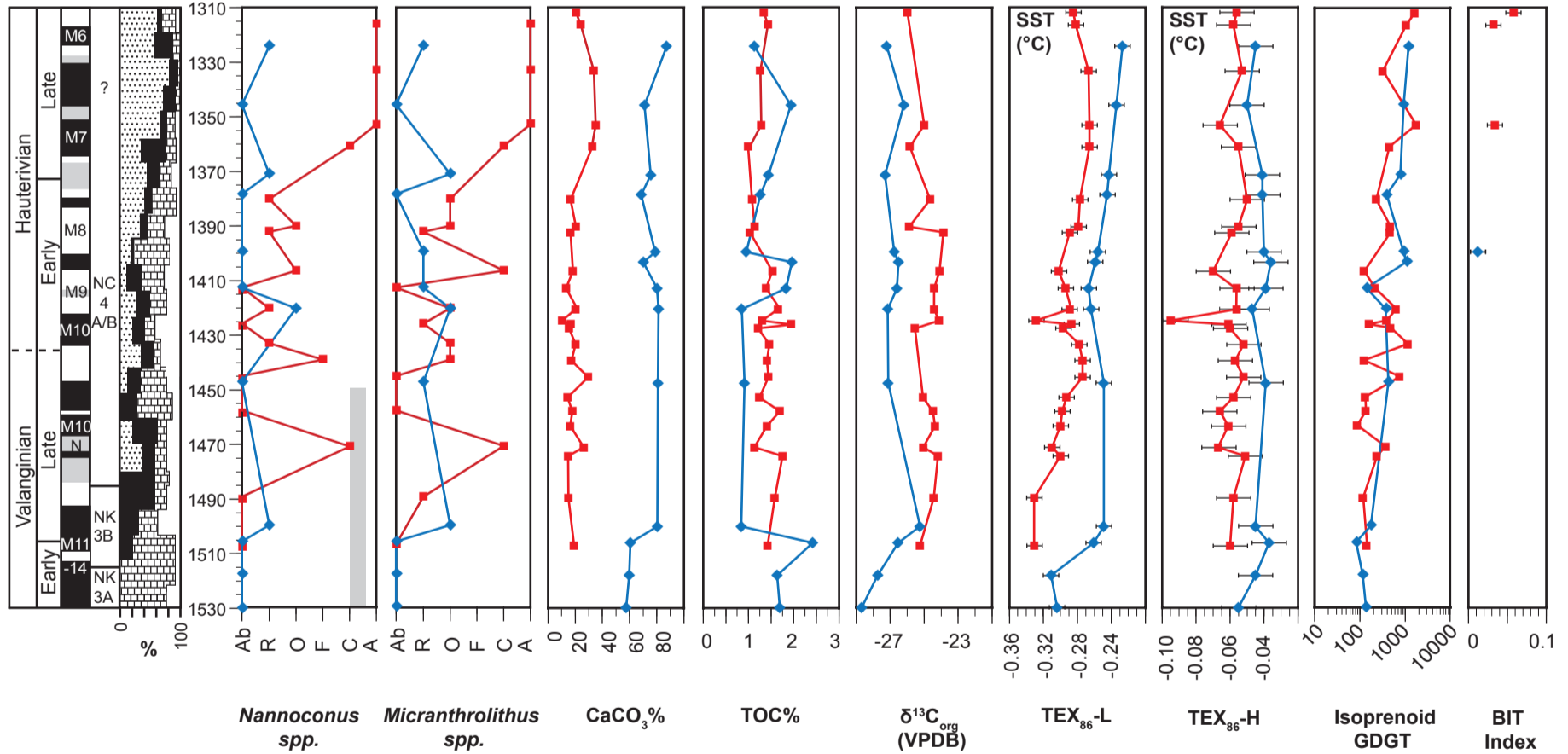
= Laminated marl   = Bioturbated chalk   = Homogeneous mudstone   = Sandstone

Isoprenoid GDGTs

Branched GDGTs

0.
1302

I.
1022

1.
1300

II.
1036

2.
1298

III.
1050

3.
1296

4.
1292

"Crenarchaeol"

4'.
1292

"Crenarchaeol isomer"
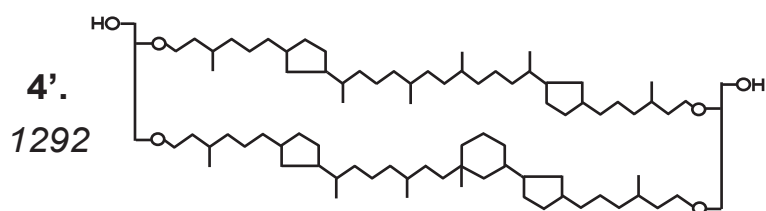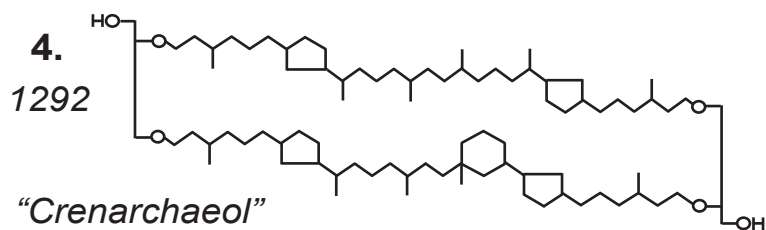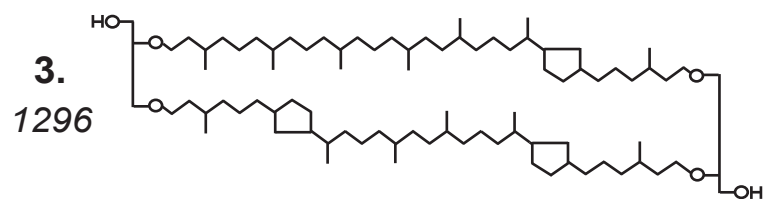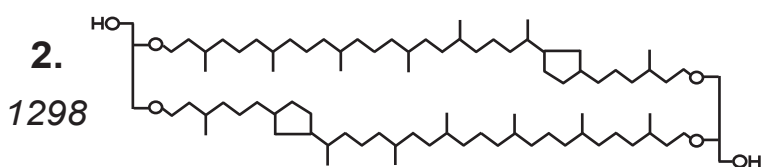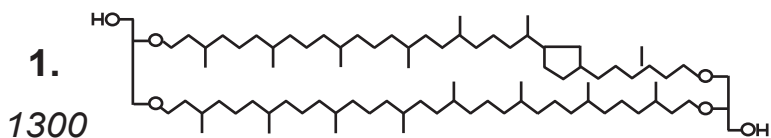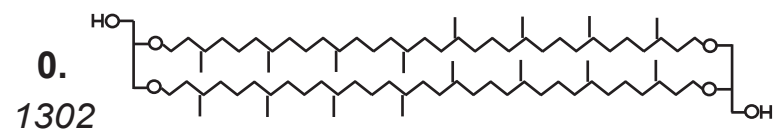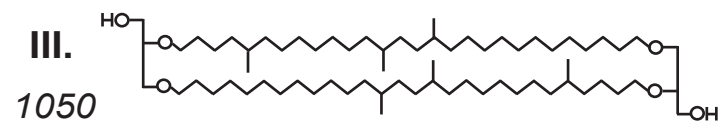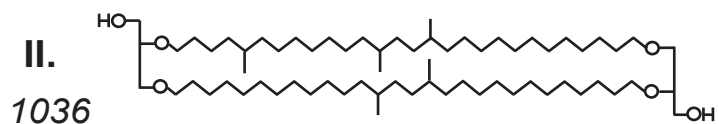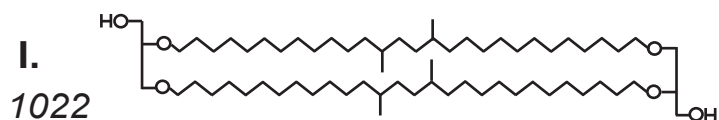
Fig. S1. The structure and nomenclature of the core GDGT molecules discussed in this paper.
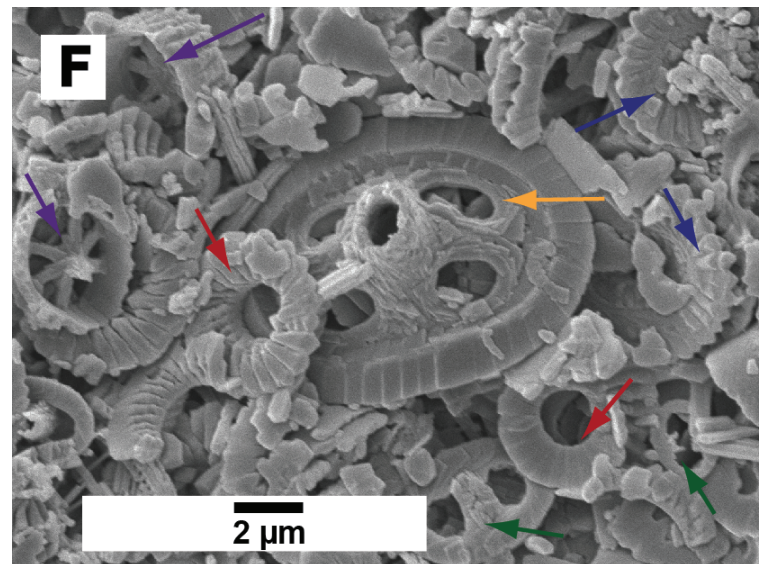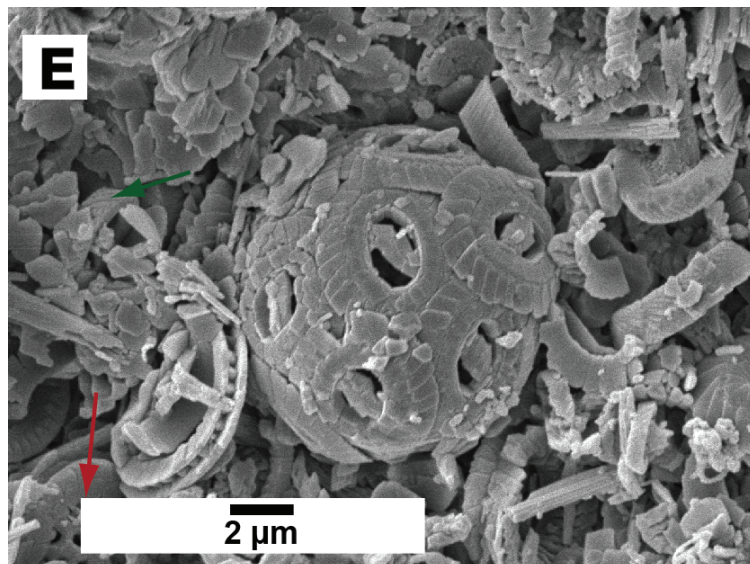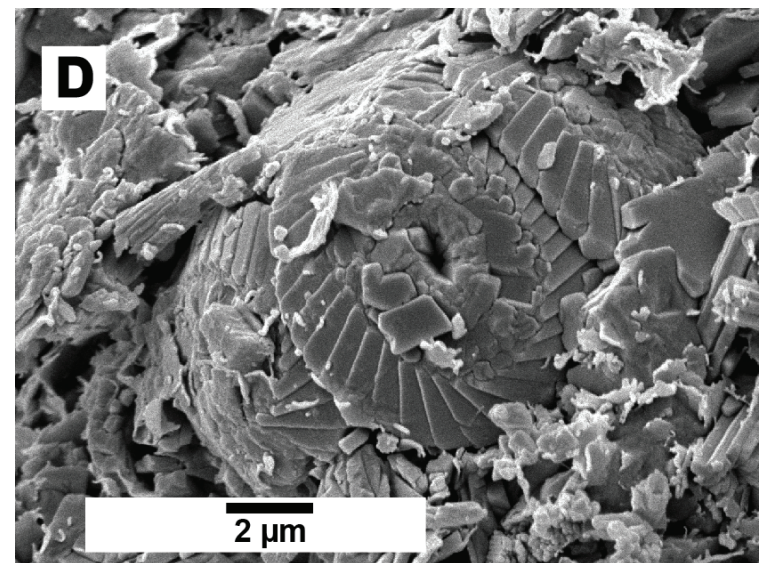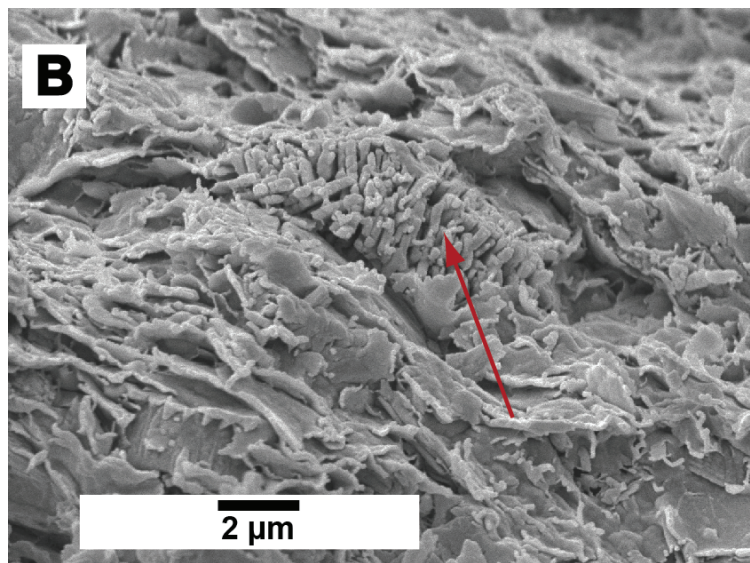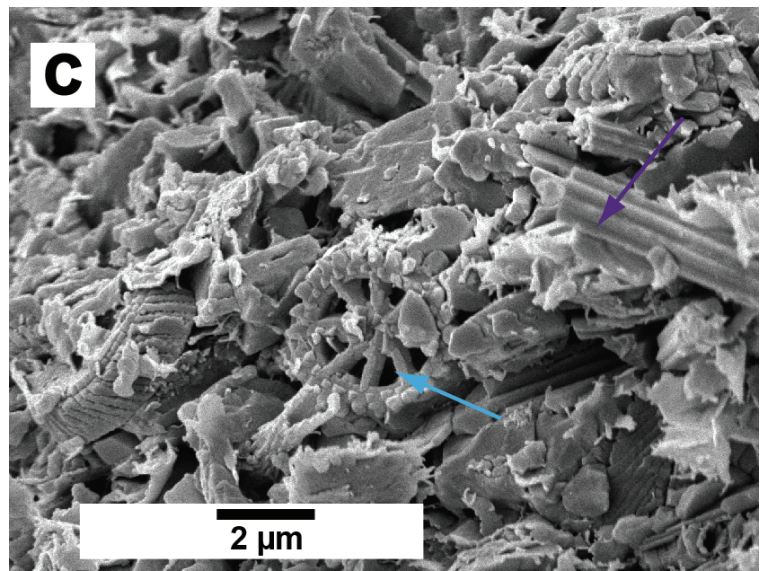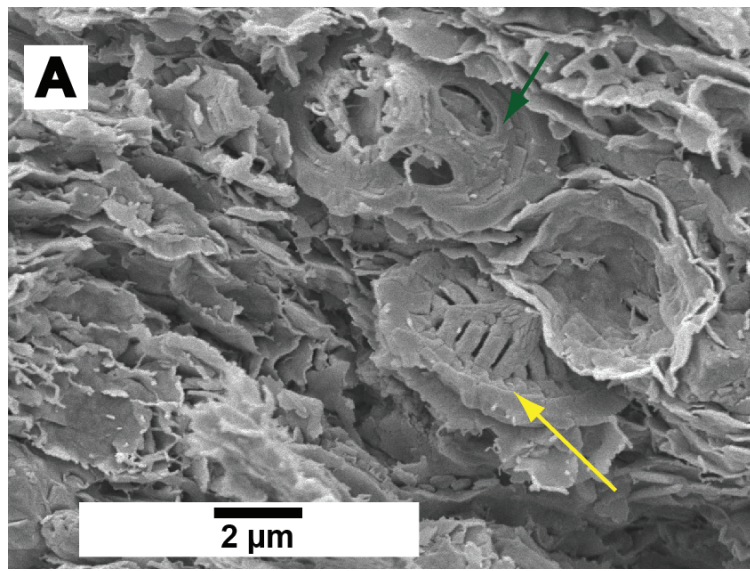
Fig. S2a. Scanning electron micrographs of rock surfaces from paired marl and mudstone samples from DSDP Site 534. A & B = DSDP 534A-60-04, 63cm; homogeneous mudstone. **A** = X 7,500 mag. Clay-rich layer containing well-preserved coccoliths. A *Cretarhabdus madingleyensis* is indicated by a yellow arrow, showing fine central structures,and a somewhat etched *Axopodorhabdus dietzmanii* is indicated by green arrow. **B** = X 7,000 mag. Clay flakes and a *Nannoconus* sp. **C & D** = DSDP 534A-60-04, 66cm; laminated marl. **C** = X 8,000 mag. Well-preserved coccoliths and clay flakes. *Lithraphidites carniolensis* is common throughout (purple arrow) and *Rotelapillus laffittei* (pale blue arrow) is quite common and shows good preservation of the delicate central bars. **D** = X 8,000 mag. *Watznaueria barnesiae* coccosphere. Some secondary calcite is visible, but coccoliths are generally well-preserved. **E & F** = DSDP 534A-69-05, 34 cm; laminated marl. **E** = X 5,500 mag. Well-preserved *Watznaueria* sp. coccosphere, surrounded by *W. barnesiae* and *Diazomatolithus lehmanii* fragments. *Cretarhabdus conicus* visible in bottom left (red arrow), and small *Zeugrhabdotus* spp. (green arrow) to the left. **F** = X 6,000 mag. Well-preserved coccoliths including *Axopodorhabdus dietzmanii* (yellow arrow), with *D. lehmanii*, (red arrows), with *W. barnesiae* (blue arrows), *Stradnerlithus geometricus* (purple arrows) and two different *Zeugrhabdotus* spp. (green arrows).
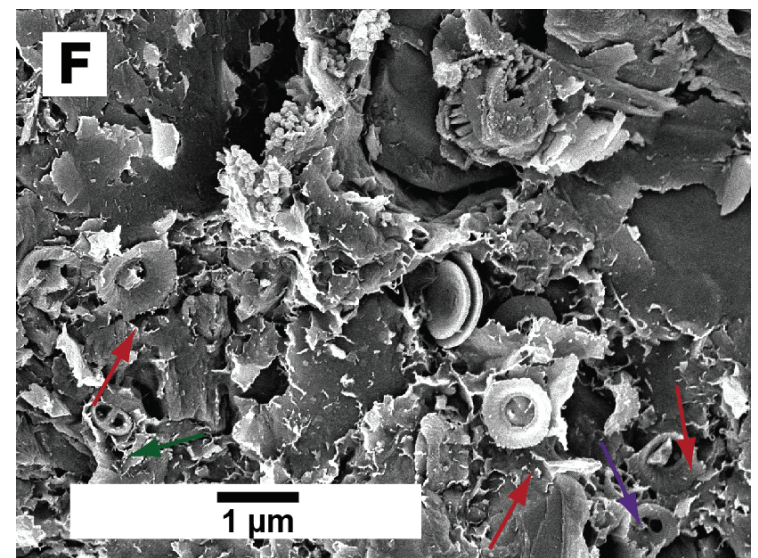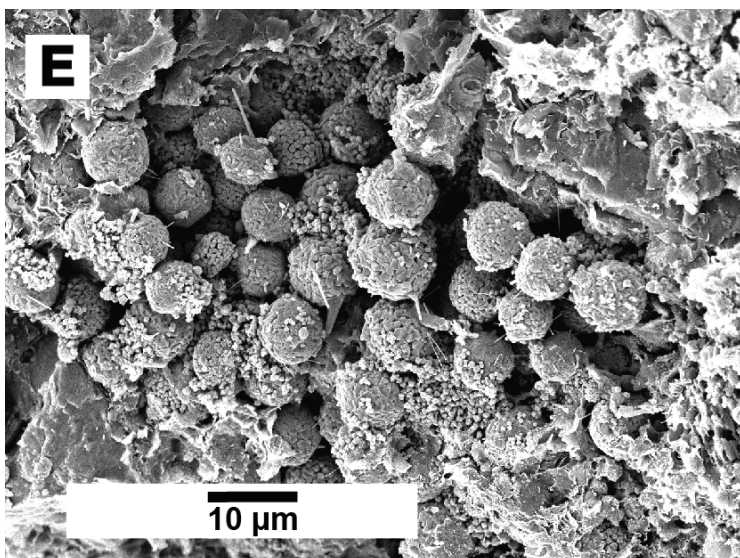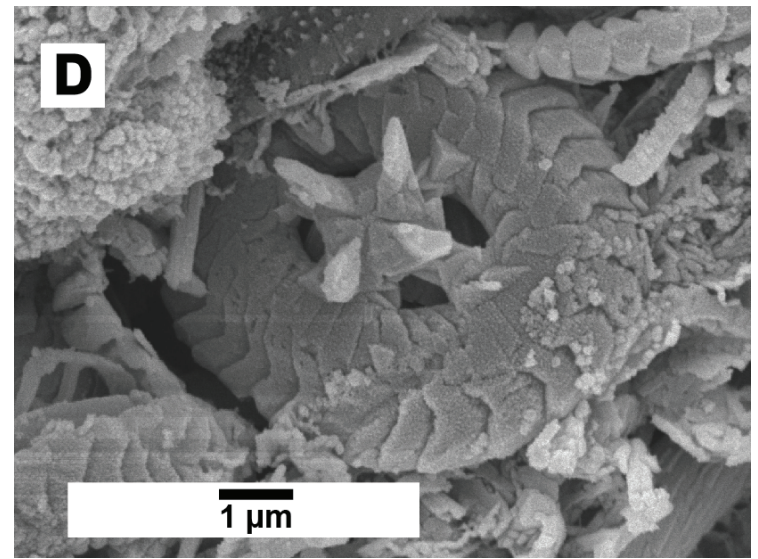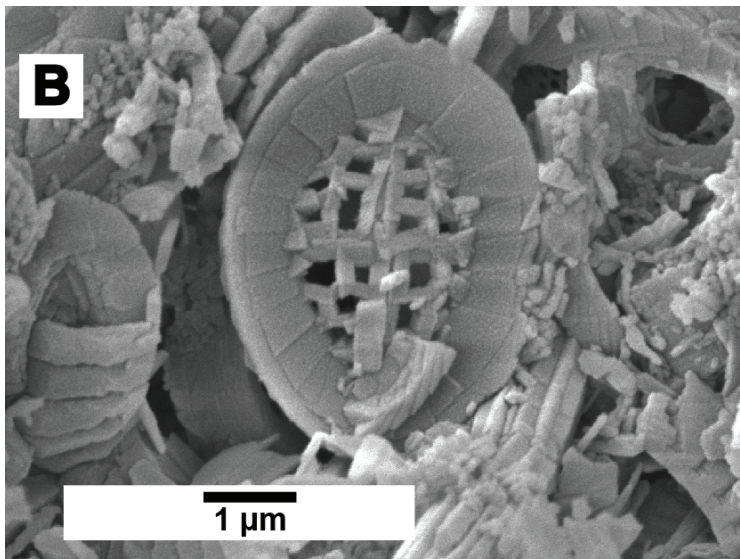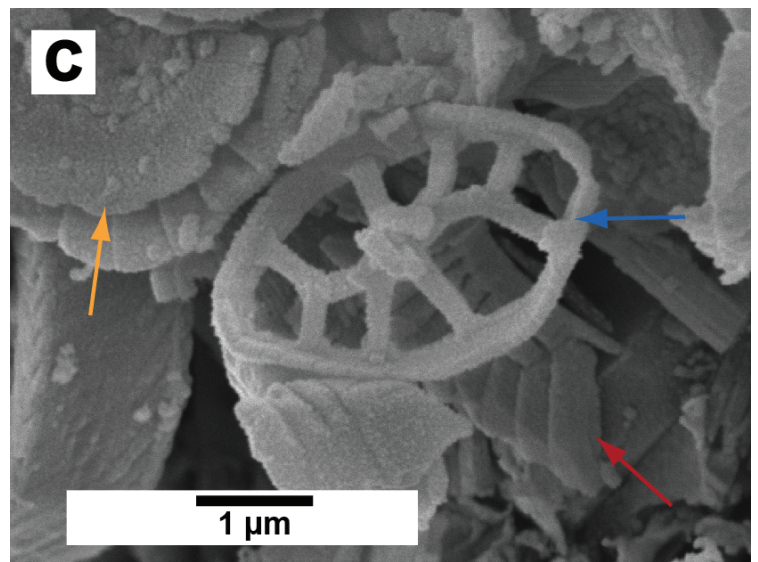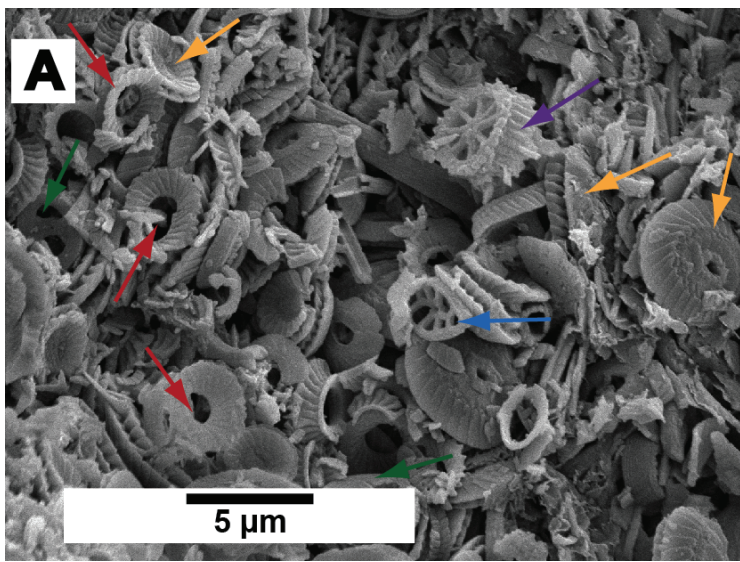
Fig. S2b. Scanning electron micrographs of rock surfaces from sample DSDP 603B-57-5, 49 cm (**ABCD**); laminated marl, excellent preservation. **A** = X 4,300 mag. Dominated by very well-preserved calcareous nannofossils, including *W. barnesiae* (yellow arrows), *D. lehmanii* (red arrows), *Zeugrhabdotus* spp. (green arrow), *R. laffittei* (purple arrow), *Stradnerlithus asymmetricus* (blue arrow). **B** = X 16,000 mag. *Cretarhabdus inaequalis* showing well-preserved central grill structure. **C** = X 4,300 mag. Well-preserved *Stradnerlithus asymmetricus* (blue arrow) surrounded by *Biscutum constans* (yellow arrow) and *D. lehmanii* (red arrow). **D** = X 13,000 mag. Well-preserved *Helenea chiastia*. **E & F** = DSDP 603B-75-03, 85 cm; homogeneous mudstone. **E** = X 1,500 mag. A cluster of pyrite framboids surrounded by clay flakes. **F** = X 2,700 mag. Clay containing moderately-preserved calcareous nannofossils, including *D. lehmanii* (red arrows) and a small *Zeugrhabdotus* spp. (green arrow).
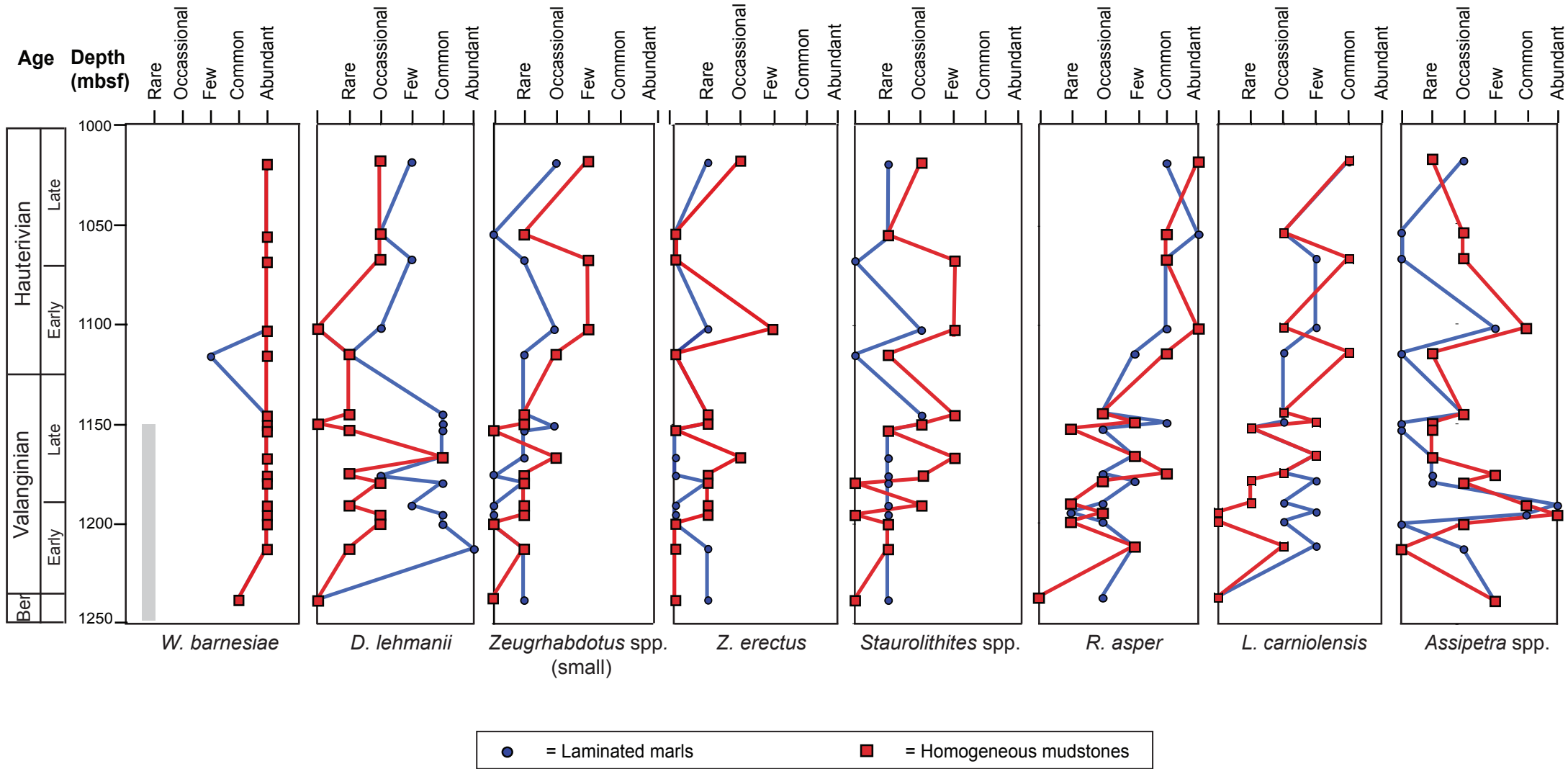
Fig. S3. Calcareous nannofossil data from DSDP Site 534, showing abundance data from selected species and genera. Grey bar indicates approximate span of the 'nannoconid crisis' after Erba et al., 2004, which is also associated with a peak in *D. lehmanii* in Tethyan sections.

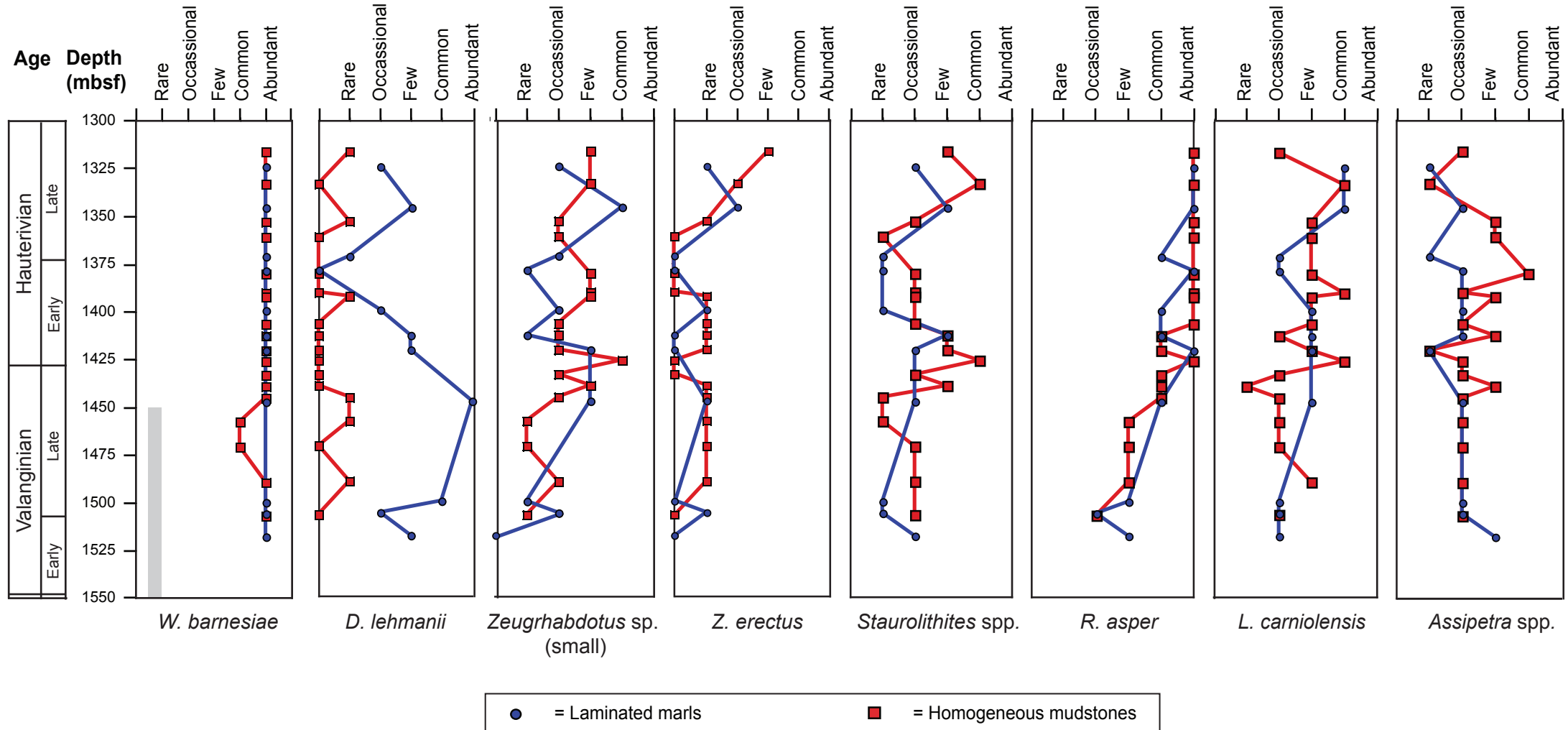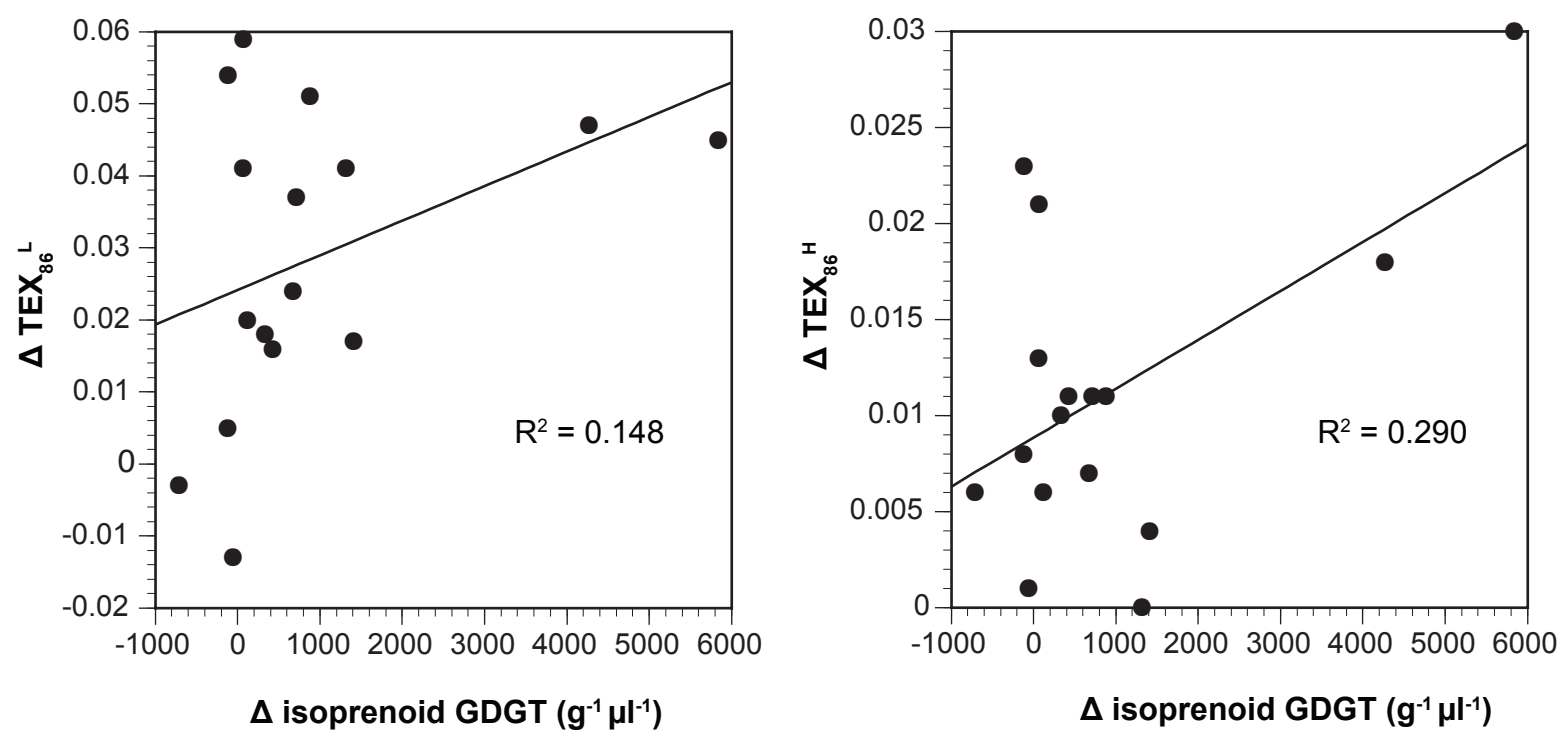**DSDP Site 603; calcareous nannofossil abundances**

Fig. S4. Calcareous nannofossil data from DSDP Site 603, showing abundance data from selected species and genera. Grey bar indicates approximate span of the 'nannoconid crisis' after Erba et al., 2004, which is also associated with a peak in *D. lehmanii* in Tethyan sections.
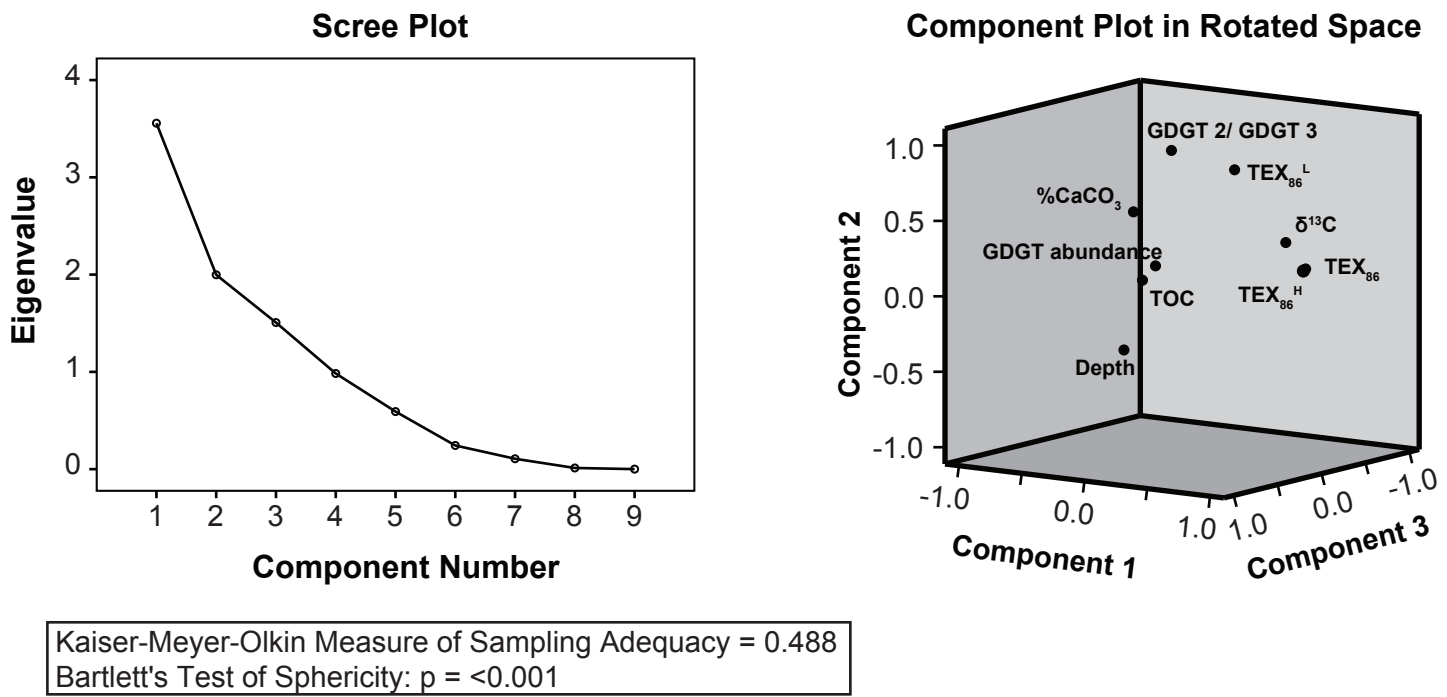
Fig. S5. a) Cross-plots for data from DSDP Site 534. The difference (Δ) between each individual lithology pair (a mudstone and a marl from a similar depth in the core), in terms of TEX_{86} ratios and isoprenoid GDGT concentrations (normalised to 1 g of dry bulk sediment and 1 µl of solvent injected onto the LC column, and to the GDGT abundance of the internal standard), are cross-plotted to show the lack of relationship; i.e., the difference in GDGT concentration between the mudstone and the marls is not causing the offset in TEX_{86} values, regardless of calibration. Simple linear regressions are shown and quantified with R^2 values. **b)** PCA analysis carried out in SPSS. Scree plot and component plot for the 9 variables that characterize the Site 534 samples (difference between marls and mudstones in terms of: depth, TEX_{86}, TEX_{86}^L, TEX_{86}^H, GDGT abundance, GDGT-2 / GDGT-3 ratio, %TOC, %$CaCO_3$, and $\delta^{13}C$). The Kaiser-Meyer-Olkin Measure of Sampling Adequacy is below the 0.6 threshold, suggesting this dataset does not pass the assumptions required for PCA analysis. Additionally, no principle components could be identified at the rotated component matrix stage, and no clustering is obvious from the component plot, suggesting no strong underlying relationship between the various geochemical variables.